

ARTICLE

Degradation of dendritic cargos requires Rab7-dependent transport to somatic lysosomes

Chan Choo Yap¹, Laura Digilio¹, Lloyd P. McMahon¹, A. Denise R. Garcia², and Bettina Winckler¹

Neurons are large and long lived, creating high needs for regulating protein turnover. Disturbances in proteostasis lead to aggregates and cellular stress. We characterized the behavior of the short-lived dendritic membrane proteins Nsg1 and Nsg2 to determine whether these proteins are degraded locally in dendrites or centrally in the soma. We discovered a spatial heterogeneity of endolysosomal compartments in dendrites. Early EEA1-positive and late Rab7-positive endosomes are found throughout dendrites, whereas the density of degradative LAMP1- and cathepsin (Cat) B/D-positive lysosomes decreases steeply past the proximal segment. Unlike in fibroblasts, we found that the majority of dendritic Rab7 late endosomes (LEs) do not contain LAMP1 and that a large proportion of LAMP1 compartments do not contain CatB/D. Second, Rab7 activity is required to mobilize distal predegradative LEs for transport to the soma and terminal degradation. We conclude that the majority of dendritic LAMP1 endosomes are not degradative lysosomes and that terminal degradation of dendritic cargos such as Nsg1, Nsg2, and DNER requires Rab7-dependent transport in LEs to somatic lysosomes.

Introduction

Protein homeostasis is essential to cellular health in all cell types. Because neurons are both postmitotic and long-lived, maintaining the proteome is of particular importance. Not surprisingly, disturbances in protein turnover in neurons have been associated with numerous neurodegenerative disorders as well as aging (Douglas and Dillin, 2010; Cornejo et al., 2017). Neurons are also extraordinarily large cells whose processes—axons and dendrites—can span hundreds of micrometers or more. How protein turnover is regulated in time and space in axons and dendrites is thus an essential cell biological question (Jin et al., 2017).

Nsg1 (NEEP21) and Nsg2 (P19) are neuron-specific small transmembrane proteins found in dendritic endosomes. Nsg1 has been implicated in regulating the trafficking of multiple neuronal receptors (Steiner et al., 2005; Yap et al., 2008; Norstrom et al., 2010). Mistargeting of these receptors after knockdown of Nsg1 resulted in shorter axon growth on L1 substrate (Lasiecka et al., 2014), impaired long-term potentiation in hippocampal slices (Alberi et al., 2005), and increased amyloidogenic processing of β APP (Norstrom et al., 2010). We recently discovered that Nsg1 and Nsg2 are short lived in neurons (Yap et al., 2017). The rapid degradation of Nsg proteins allows us to ask where dendritic membrane proteins are degraded and how their degradation is regulated because changes in protein levels can easily be detected in interference experiments.

In fibroblasts, endosomal populations and their maturation are well studied, and several markers are routinely used to distinguish early endosomes (EEs; EEA1) from late endosomes (LEs) and lysosomes (Rab7/LAMP1). In fact, the overlap of Rab7 with LAMP1 is so extensive in fibroblasts (>75%; Humphries et al., 2011; Hubert et al., 2016) that LEs and lysosomes are often combined into a single “LE/lysosome” category. Using the same markers and functional assays routinely used in fibroblasts, we undertook a comprehensive categorization of endosomes in dendrites. We discovered a steep spatial gradient of endosomes along dendrites: EEs and LEs are abundant throughout dendrites, whereas the abundance of degradative acidified lysosomes declines rapidly with increasing distance from the soma both ex vivo and in vivo. Second, we discovered that dendrites contain distinct Rab7⁺ compartments which we term “early” LEs and “late” LEs depending on whether LAMP1 is present or not. Unlike in fibroblasts, Rab7 compartments in dendrites frequently lack LAMP1, are not acidified, and do not contain the abundant lysosomal proteases cathepsin (Cat) B or D. Third, we show that long-range Rab7-dependent dendritic transport back to the proximal dendrite and soma (retrograde) is required for degradation, indicating that the degradative capacity of the more distal dendritic segments is not sufficient for terminal degradation. We propose that terminal degradation of dendritic membrane proteins occurs

¹Department of Cell Biology, University of Virginia, Charlottesville, VA; ²Department of Biology, Drexel University, Philadelphia, PA.

Correspondence to Bettina Winckler: bwinckler@virginia.edu; Chan Choo Yap: cy5x@virginia.edu.

© 2018 Yap et al. This article is distributed under the terms of an Attribution–Noncommercial–Share Alike–No Mirror Sites license for the first six months after the publication date (see <http://www.rupress.org/terms/>). After six months it is available under a Creative Commons License (Attribution–Noncommercial–Share Alike 4.0 International license, as described at <https://creativecommons.org/licenses/by-nc-sa/4.0/>).



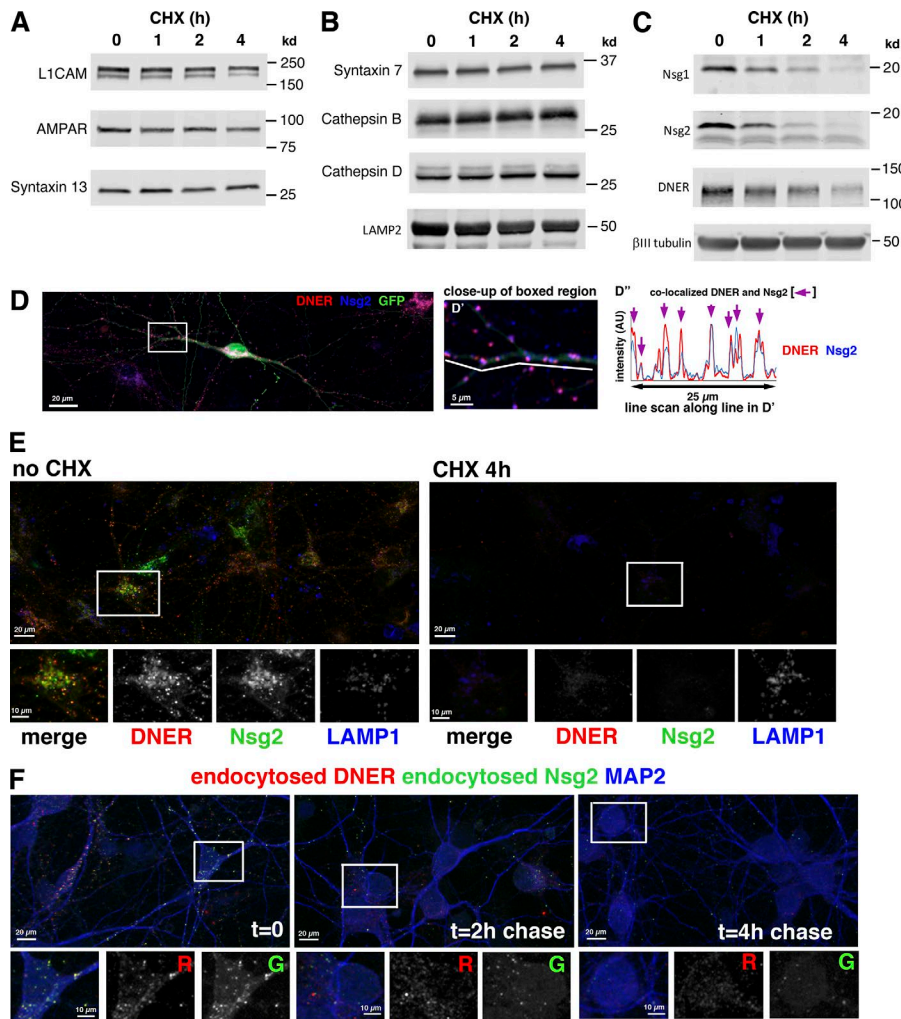


Figure 1. Nsg family proteins and DNER have short half-lives in neurons. (A–C) Protein levels from neuronal cultures were determined after 0, 1, 2, and 4 h CHX treatment. Membrane proteins associated with the plasma membrane (L1-CAM and AMPAR) and recycling endosomes (syntaxin13) were probed in A, proteins were localized to LEs and lysosomes in B, and dendritic membrane proteins with short half-lives in C. Tubulin was used as a loading control. **(D)** Endogenous DNER (red) receptor largely colocalizes with Nsg2 (blue). GFP outlines the cell shape. **(D')** The boxed region is shown as a close up. **(D'')** A line scan along the white line in D' visualizes the extent of peak coincidence of DNER and Nsg2 (purple arrows). **(E)** Cultures were incubated without CHX or with CHX for 4 h and then immunostained against endogenous Nsg2 (green), DNER (red), LAMP1 (blue), and MAP2 (not depicted). The boxed region is shown below as merged and single channels. DNER and Nsg2 levels but not LAMP1 levels were greatly decreased after 4 h CHX treatment. Representative images are shown from one experiment out of a total of five independent repeats. **(F)** Degradation of DNER and Nsg2 after endocytosis. Endocytosis of Nsg2 (green) and DNER (red) was performed, and cultures were fixed either immediately ($t = 0$) or after 2 or 4 h chase at 37°C. One cell is boxed and shown below as merged and single channels. G, green; R, red. MAP2 is counterstained to identify neurons (blue).

overwhelmingly in somatic lysosomes and that Rab7⁺ LEs are the primary retrograde carriers for dendritic degradative cargos.

Results

Nsg family proteins and delta notch EGF repeat-containing receptor (DNER) have short half-lives in neurons

We recently discovered that the endosomal somatodendritic transmembrane proteins Nsg1 and Nsg2 (collectively referred to as Nsg proteins) have short half-lives of ~90 min in cultured neurons (Yap et al., 2017). We first investigated whether proteins that have been linked functionally to Nsg1 (i.e., L1, α -amino-3-hydroxy-5-methyl-4-isoxazolepropionic acid receptor [AMPA], and the EE/recycling endosome-resident SNARE protein syntaxin13) are similarly short lived. Protein levels were quantified in cultured neurons treated with cycloheximide (CHX) for ≤ 4 h. For L1, AMPAR (GluA2), and syntaxin13, remaining protein levels ranged from ~70 to 80% after 4 h CHX (Fig. 1 A). 90% or more protein remained for the LE SNARE syntaxin7 and the lysosomal proteases CatB and CatD (Fig. 1 B). The levels of the lysosome-associated membrane protein LAMP2 remained at ~80% after 4 h in CHX (Fig. 1 B). In striking contrast, levels of Nsg1 and Nsg2 were reduced to <20% by 4 h (Fig. 1 C; Yap et al., 2017).

Proteomic research previously revealed that both Nsg1 and the dendritic membrane receptor DNER accumulated highly in CatB/L double-knockout mice, suggestive of high turnover rates (Stahl et al., 2007). DNER indeed had a short half-life of ~2.5 h in hippocampal neurons (Fig. 1 C). Endogenous DNER was localized to puncta in the soma and dendrites, consistent with previous work (Eiraku et al., 2002, 2005). Nsg2 localized primarily to EEs and LEs in dendrites (Yap et al., 2017), and DNER colocalized to the same compartments (Fig. 1 D).

To more directly compare the turnover rates of LAMPs, Nsg, and DNER specifically in neurons, we used immunofluorescence (IF) microscopy and identified neurons by MAP2 counterstaining. Large differences of protein stability in the presence of CHX between endogenous Nsg2, DNER, and LAMP1 were also observed with this assay (Fig. 1 E): LAMP1 staining remained easily detectable after 4 h CHX, whereas both Nsg2 and DNER levels were greatly reduced. Endocytosis assays using antibodies against the extracellular domain of endogenous DNER revealed that the levels of endocytosed DNER were greatly decreased after a 4-h chase (Fig. 1 F), similar to simultaneously endocytosed Nsg2. DNER is thus also an itinerant rather than a resident endosomal protein, which travels to lysosomes for rapid degradation after endocytosis.

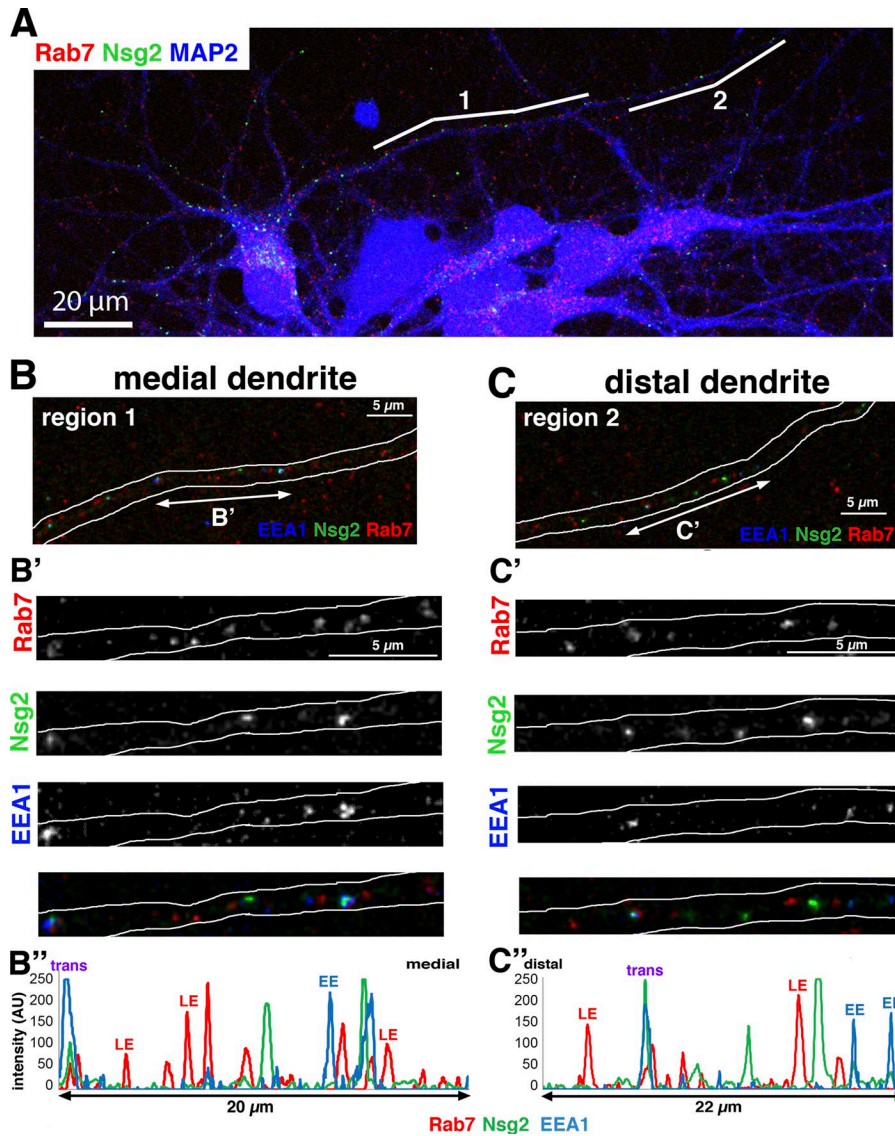


Figure 2. Rab7, EEA1, and Nsg2 are present along dendrites. (A–C) DIV 7–8 hippocampal neurons were stained against MAP2 (to mark dendrites), EEA1, Nsg2, and Rab7 (all endogenous). The channel colors are indicated for each panel. (B and C) Regions marked 1 and 2 in A are shown as close ups in B (medial dendrite, region 1) and C (distal dendrite, region 2). MAP2 staining was used to outline the dendrite in white. A close up of the segments marked by double-headed arrows in B and C are shown as individual channels in B' and C'. (B'' and C'') Line scans of the dendritic segment in B' and C'. Positively staining endosomes for all three markers can be observed all along the dendrite. As examples, some of the peaks are annotated as EEs (EEA1 positive/Rab7 negative), LEs (EEA1 negative/Rab7 positive), and trans (transitioning EE/LE; EEA1 positive/Rab7 positive).

EEs and LEs are distributed throughout dendrites

Given the very short half-lives of Nsg proteins, we wondered whether degradation was taking place locally in dendritic lysosomes. We first determined the spatial distribution of different endosomes using the widely used markers EEA1 (EE), Rab7 (LE), and Nsg2 (EE + LE; Fig. 2, A–C). All markers stained abundant puncta in the soma but also extended a significant distance into dendrites (region 1; Fig. 2, B and B'), often being detectable >100 μm past the soma to near the distal tips (region 2; Fig. 2, C and C'). The staining intensity of many endosomes tended to decline somewhat with distance from the soma, but many bright compartments were consistently observed in the distal dendrite (Fig. 2, B' and C'). EEA1 and Rab7 showed partial colocalization (~20–30%), consistent with the notion of transitioning EEs/LEs (Rink et al., 2005; see annotated peaks in Fig. 2, B' and C').

Distinct spatial distribution of LE/lysosome markers along dendrites

Next, we determined the localization of lysosomes in dendrites using the widely used markers Rab7 and LAMP1 (Fig. 3, A–C;

Humphries et al., 2011). To more precisely identify compartments capable of degradation, we also stained against endogenous Cathepsin B (CatB), thus using a definition of lysosomes as compartments containing lysosomal cathepsins. We used the term “degradative lysosome” to designate these compartments (LAMP1 positive/CatB positive). The density (number of compartments per unit volume) and intensity profiles changed profoundly with distance from the soma and were strikingly different for CatB compared with LAMP1, Nsg2, and Rab7 (Fig. 3, B and C). To quantify the marker distribution along dendrites (Fig. 3 D), we subdivided the major dendrite into three regions from the soma boundary: proximal dendrite, 0–25 μm; juxtaproximal dendrite, 25–50 μm; and medial dendrite, 50–75 μm. Rab7- and Nsg2-containing compartments were found throughout dendrites but showed an initial drop in density between the proximal and juxtaproximal segment, and then density remained fairly stable (Fig. 3 D). LAMP1-containing compartments were present into and past the juxtaproximal dendrite but continued to become sparser medially compared with the juxtaproximal dendritic regions. In contrast, CatB staining was rare past the

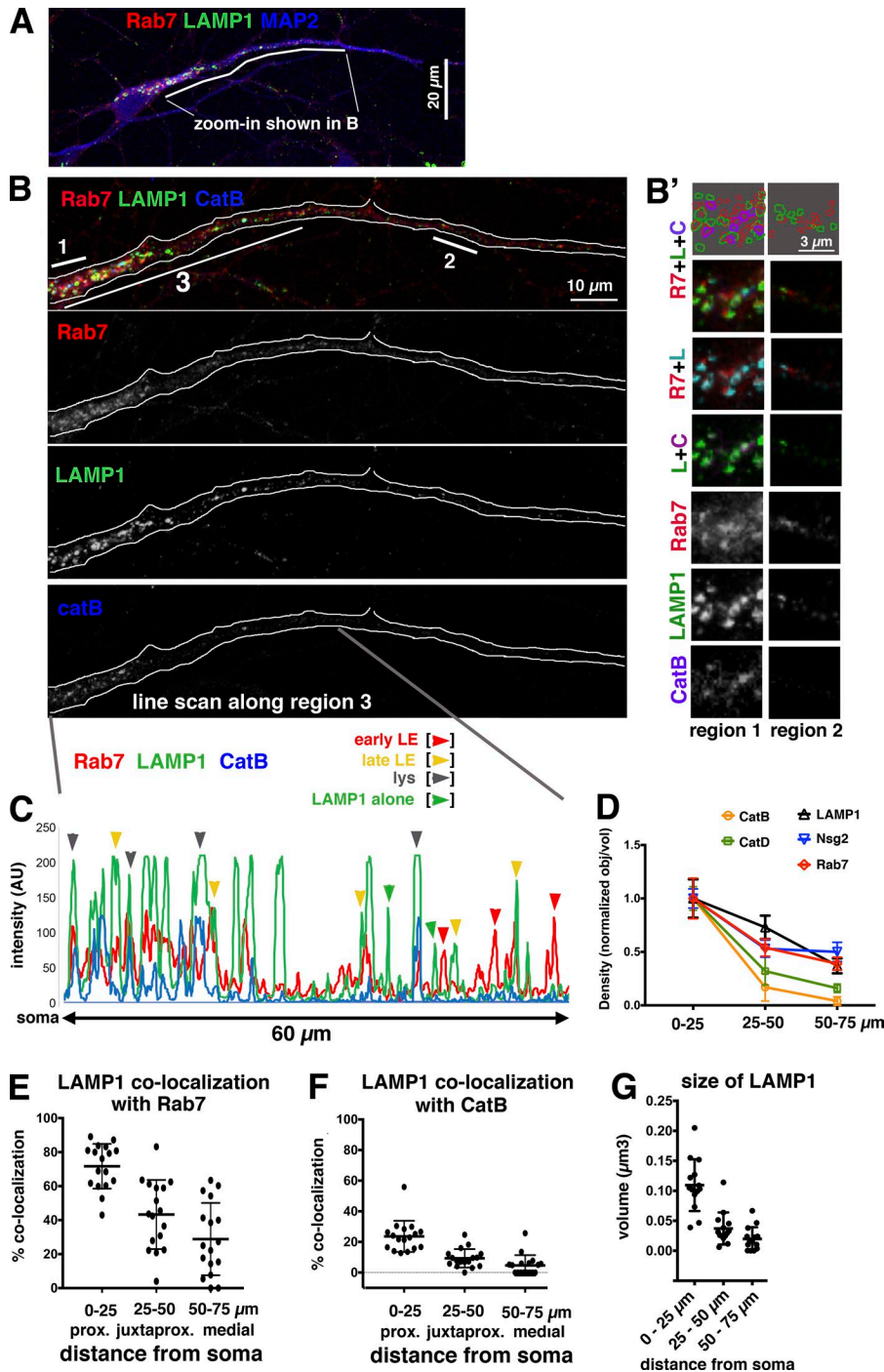


Figure 3. Differential abundance of Rab7, LAMP1, and CatB and D along dendrites. (A and B) DIV 7 hippocampal neurons were stained against MAP2 (to mark dendrites), Rab7 (R7), LAMP1 (L), and CatB (C; all endogenous). The channel colors are indicated for each panel. The first 100 μm of the largest dendrite (marked by white line in A) is shown as merged channels and single channels in B. Close ups of the regions marked 1 (proximal) and 2 (medial) are shown in B'. Single channels and merged channels are shown as indicated. A schematic representation of the compartment subtypes is shown at the top. Purple compartments indicate degradative lysosomes (LAMP1 + CatB). Green plus red compartments indicate late LEs (LAMP1 + Rab7). Red-alone compartments indicate early LEs (Rab7 but no LAMP1). Green-alone compartments indicate LAMP1-only compartments (neither LE nor lysosome). Representative images are shown from one experiment of a total of five independent repeats. (C) A line scan along region 3 (marked by the white line 3 in B) is shown. Compartment designations are indicated by arrowheads as examples. (D–G) Quantification of the distribution of endogenous endosome markers from confocal z stacks. 50 to >200 endosomes were quantified and averaged for each cell. n = confocal z stacks reconstructed from 14–17 neurons from two independent cultures. (D) The density (number of compartments per unit volume) of endosomal markers was determined with increasing distance from the soma (x axis) and subdivided into three regions: soma to 25 μm (proximal), 25–50 μm (juxtproximal), or 50–75 μm (medial) dendritic segments. Density was normalized to the proximal segment for each marker. Nonnormalized quantification is shown in Fig. S1 E. Error bars indicate SEM. (E and F) Colocalization of LAMP1 with Rab7 (E) and CatB (F) was quantified using Imaris. (G) Quantification of the apparent volume of LAMP1-positive compartments. (E–G) Error bars indicate SD.

proximal region (Fig. 3, B and B'), and many dendrites had zero CatB-positive puncta in the medial segment (Fig. 3 B', region 2). Similar to CatB, the density of CatD (Figs. 3 D and S1 E) also declined rapidly past the proximal dendritic segment. Many of the major dendrites extended distally past 75 μm and were often much longer than 100 μm . LAMP1 and CatB/D puncta were essentially absent in these distal regions and thus not included in Fig. 3 D. We note that there was a noticeable difference between dendrites of different diameters. The major (largest diameter) dendrite usually contained many CatB/D-positive compartments in the proximal segment, whereas minor dendrites usually showed little LAMP1 or CatB/D staining even proximally. EEAI,

Nsg proteins, and Rab7 were all present in minor as well as major dendrites. We thus conclude that Rab7, LAMP1, and CatB/D do not define the same compartments and cannot be used interchangeably to mark degradative lysosomes.

Early LEs (Rab7⁺/LAMP1⁻) are abundant in medial and distal dendrites

We next quantified the colocalization of LAMP1 with Rab7 and found that it decreased with increasing distance from the soma (Fig. 3 E). Because this result was unexpected given the fibroblast literature (Humphries et al., 2011; Hubert et al., 2016), we validated the Rab7 antibody in our own hands (Fig. S1, A–C). We

then determined whether the Rab7-positive/LAMP1-negative compartments in dendrites were transitioning EEs (i.e., EEA1 positive) or constituted a Rab7-positive/EEA1-negative/LAMP1-negative compartment. Because of antibody incompatibility, we had to overexpress Rab7 for this marker combination (Fig. S2, A and B). In the soma, Rab7-GFP greatly colocalized with LAMP1. In contrast, Rab7-GFP compartments in the distal half of dendrites frequently contained neither EEA1 nor LAMP1. We categorized these EEA1-negative/Rab7-positive/LAMP1-negative endosomes as “early” LEs (Fig. S2 C, green arrows). We also observed a sizable proportion of LAMP1 compartments in the medial/distal dendrites, which lacked Rab7, EEA1, and CatB. The exact identity of these compartments (LAMP1 alone) was not clear (Fig. 3 C, line scan).

LAMP1⁺ endosomes in dendrites rarely contain CatB or D

LAMP1-positive compartments in the soma and proximal portion of major dendrites colocalized substantially (but partially) with CatB (Fig. 3 F), making them degradative lysosomes. Whereas all CatB-positive compartments contained LAMP1, LAMP1-positive compartments >25 μm from the soma boundary rarely contained CatB (Fig. 3 F). These dendritic LAMP1-containing compartments thus might be nondegradative “late” LEs rather than degradative lysosomes. In addition, the volume of the LAMP1-stained compartments decreased strikingly past the first 25 μm from the soma (Fig. 3 G). The large LAMP1 compartments appeared doughnut-shaped by high-resolution confocal microscopy (Fig. S2 D, arrowheads). LAMP1 compartments more distally in dendrites were small, and a lumen could not be resolved (Fig. S2 D, arrows). We thus discovered a spatial gradient of endosomal compartments in dendrites with EEs (EEA1 positive) and LEs (Rab7 positive) extending far into the distal portion of dendrites, and compartments containing lysosomal proteases (LAMP1 positive/CatB/D positive) being concentrated in the soma and the proximal portion of dendrites.

Lysosomes are rarely found in distal dendrites of mature neurons

We then asked whether degradative lysosomes showed a steep spatial gradient in more mature neurons as well. We stained surface GluA1 to visualize dendrites and spines in day in vitro (DIV) 60 hippocampal neurons and counterstained with LAMP1 and CatB (Fig. 4, A and A'). LAMP1 could be detected brightly in the soma and proximal dendrite. Smaller, fainter LAMP1 compartments were also observed more distally, but they largely lacked CatB (red arrowheads in Fig. 4 A'). We occasionally detected LAMP1 in a spine close to the soma (similar to Goo et al., 2017; Padamsey et al., 2017), but CatB staining was not apparent in spines.

Next, we imaged endogenous LAMP1 and CatB in sparsely GFP-labeled coronal cryosections of P28 mouse cortex using the Thy1-EGFP M line. Neurons whose apical dendrites were largely contained within a cryosection were imaged by confocal microscopy (Fig. 4, B and B'). LAMP1-containing compartments were abundant in the soma and proximal dendrite. The extent to which LAMP1 could be detected more distally was variable in different cells. Similarly to cultured neurons, LAMP1-positive

compartments past the proximal region were smaller than somatic and proximal LAMP1 compartments. CatB-containing compartments were also abundant in the soma, but then they greatly decreased with increasing distance from the soma in all dendrites we observed. CatB was rarely detected in the more distal portions of the dendrite (regions 2 and 3), and substantial lengths of the medial/distal dendrite contained no compartments containing CatB (Fig. 4 B', purple arrow shows rare positive compartment). A model of endosomal progression (indicating marker abundance and the compartment designations) is diagrammed in Fig. 4 C (in time) and Fig. 4 D (in space).

Dendrites mostly lack acidified lysosomes containing active cathepsins

We next used two operational assays to define degradative lysosomes: LysoTracker to stain acidified compartments and MagicRed (MR)-cathepsin substrates (MR-Cat) to stain compartments with active cathepsins. GFP expression was used to visualize cell shape. Both LysoTracker (Fig. 5 A) and MR-CatB (Fig. 5 B) were present abundantly on brightly stained compartments in the soma and proximal portion of the major dendrites. Further out in the dendrites, small and faint compartments were occasionally found (arrowheads in right panels). In addition, we visualized dendritic endosomes by expressing Nsg1-Em and imaged with LysoTracker Red or MR-CatB (Fig. S3). Many of the Nsg1-Em-containing endosomes near the soma were brightly stained with LysoTracker or MR-CatB, but the tracer staining became very faint in Nsg1-Em endosomes past the proximal segment and less abundant overall (Fig. S3, A' and B'). LysoTracker and MR-CatB stained strongly in nonneuronal cells present in our cultures.

To distinguish degradative lysosomes (defined as simultaneously acidified and degradative) from predegradative LEs operationally, we performed triple live imaging with neurons expressing Rab7-BFP and labeled with Lysogreen and MR-CatB (Fig. 5, C-E). Because we were not able to determine simultaneously whether LAMP1 was present as well, we could not distinguish early and late LEs in the live imaging. Many Rab7-BFP-containing compartments did not stain with either Lysogreen or MR-CatB (blue arrows in Fig. 5 D). We categorize these Rab7 endosomes operationally as predegradative LEs (i.e., nonacidified and nondegradative). As expected, MR-positive compartments were acidified (Lysogreen positive; arrowheads in Fig. 5 E), allowing their identification as degradative lysosomes.

Because lysosomes contain many other cathepsins, we additionally labeled live neurons with MR-CatL and MR-CatK. Staining intensity along dendrites also showed a steep decline with increased distance from the soma (Fig. S3, C and D), demonstrating that multiple cathepsins all showed a similar steep spatial gradient along dendrites. Even though CatK is mostly associated with expression in bone and a neuronal transcriptome database (<http://www.brainrnaseq.org/>) lists very low CatK transcript levels in neurons, a CatK knockout mouse has central nervous system defects, and in situ show expression in the brain, including in neurons (Dauth et al., 2011). The functional assays thus led to the same conclusion as the antibody staining, namely that acidified compartments containing active cathepsins (i.e., degradative lysosomes) were found mostly in the soma and proximal

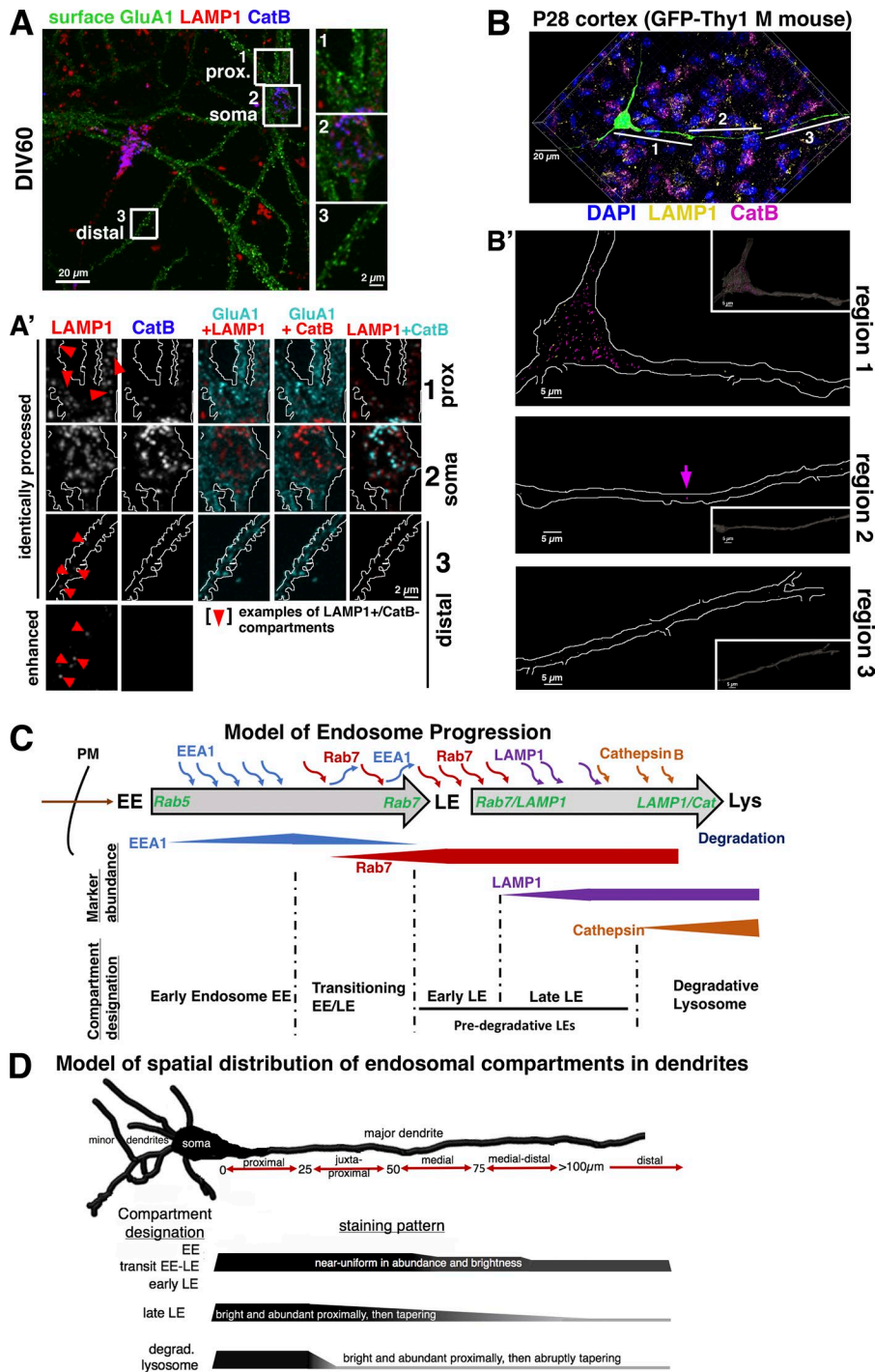


Figure 4. Distal portions of dendrites overwhelmingly lack CatB-containing lysosomes in mature cultured neurons and in mouse cortex. (A) Neurons cultured for 60 d were surface stained against endogenous GluA1 (green), LAMP1 (red), and CatB (blue). Boxes encompassing the proximal dendrite (1), the soma (2), and a distal dendrite segment (3) are indicated and shown in the close up on the right. Single-channel images and combinations of two channels are shown for the three boxed regions in A'. Channel colors are marked. Red arrowheads point at compartments positive for LAMP1 but negative for CatB. Region 3 is shown with an enhanced exposure to make faint LAMP1 compartments visible. CatB is not detectable in these compartments. (B) Coronal cryosections from the P28 cortex of GFP-Thy1 M mouse brains were stained against endogenous LAMP1 (yellow), CatB (pink), and DAPI (blue). The three regions (1–3) marked are shown as reconstructed 3D-rendered single-channel images in B'. GFP staining was used to mask the dendrite volume (inset). LAMP1-positive (yellow) and CatB-positive (pink) endosomes contained within the GFP-positive dendrite are displayed. The arrow indicates the position of a lysosome present past the proximal dendrite. (C) Model of endosome progression in time. Gradual association and dissociation of endosomal components is indicated by curved arrows. The changing abundance of each marker is shown with wedges. Dashed lines demarcate which marker combinations were designated by distinct compartment names. PM, plasma membrane. (D) Model of spatial distribution for distinct endosomal compartments. Diagram of major dendrite with the distance nomenclature indicated along red arrows below. Compartment identities and their spatial appearance are indicated. Three distinct spatial distribution patterns can be observed.

portion of the major dendrite, were sparsely present in the juxtaproximal dendrite, and were mostly absent from medial and distal dendrites.

Degradative capacity shows a spatial gradient in dendrites

Because lysosomes contain many proteases other than cathepsins, we used DQ-BSA as a general bulk degradative cargo. DQ-BSA is endocytosed and turns red upon reaching a degradative compartment (Fig. 5 F). Simultaneous incubation with Leupeptin (Leu) almost completely prevented the appearance of red fluorescence (Fig. 5 G), suggesting that Leu-sensitive proteases are the major

enzymes degrading bulk cargos such as BSA in hippocampal neurons. Neurons were then incubated with Alexa Fluor 647-BSA (to label all endosomes) and DQ-BSA for 2 h (Fig. 5, H and I). Red fluorescence was brightly visible in the soma and the proximal dendrite and rapidly tapered in abundance and intensity after the proximal segment. Alexa Fluor 647-BSA, in contrast, could be detected throughout the dendrite (Fig. 5 I).

To determine the relative degradative capacity along dendrites, we quantified the ratio of proteolytically converted DQ-BSA to total endocytosed BSA (i.e., Alexa Fluor 647-BSA) along the length of the major dendrite in ~550 endosomes from

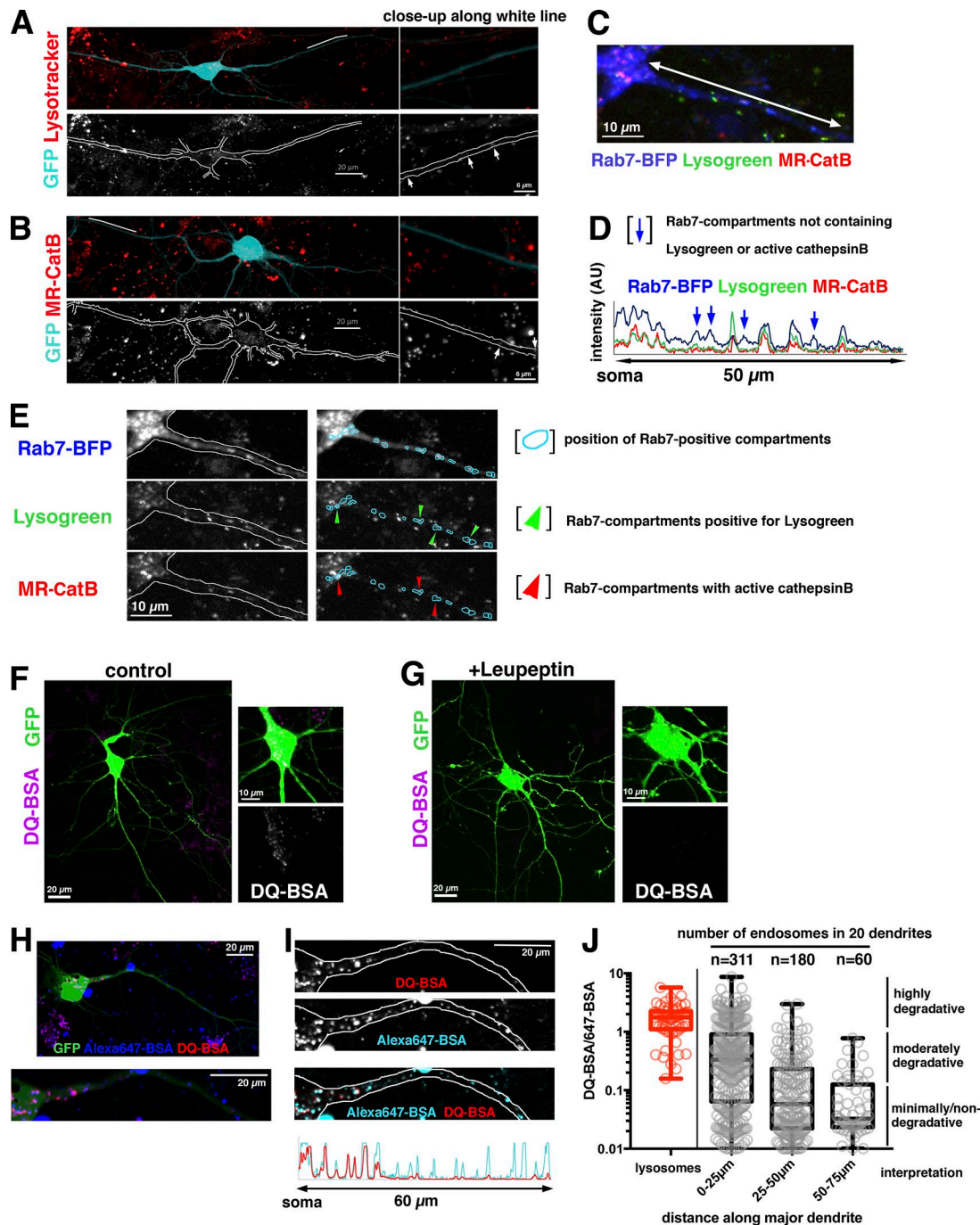


Figure 5. Medial/distal portions of dendrites mostly lack acidified, cathepsin-containing lysosomes. (A and B) DIV 9 neurons were transfected with GFP to show cell morphology. Cultures were imaged live with LysoTracker Red (A) or MR-CatB substrate (B). The red channel is shown at the bottom. The regions indicated by white lines are shown as close-ups on the right. Arrows point at the occasional tracer-containing compartments present more distally. Representative images from one experiment of at least three independent repeats are shown. **(C–E)** Acidification and presence of active CatB was simultaneously imaged by incubating DIV 9 neuronal cultures with Lysogreen (green) and MR-CatB (red) after transfection with Rab7-BFP (blue) to mark LEs in live cells. **(D)** Line scan along the double-headed arrow in C. Blue arrows indicate nonacidified, CatB-inactive, Rab7-positive endosomes. **(E)** Single channels of the cell in C are displayed (left). Rab7-BFP-positive LEs are encircled (aqua) and overlaid over each channel to allow comparison of staining (right). Rab7-BFP-positive endosomes that also contain Lysogreen or MR-CatB are indicated by green and red arrowheads, respectively. **(F and G)** Visualization of degradative compartments using DQ-BSA. Internalized DQ-BSA turns red in degradative compartments (F, purple). Incubation with Leu prevents conversion to red fluorescence (G). The soma of transfected cells are shown on the right. The DQ-BSA channel is shown alone for comparison. **(H and I)** Alexa Fluor 647-BSA (blue) was used to visualize all compartments containing BSA. DQ-BSA visualized degradative compartments (red). GFP shows the outline of the cell. Single channels and the corresponding line scan are shown on the right (I). **(J)** The ratio of DQ-BSA (degradative) to Alexa Fluor 647-BSA (total) was determined for lysosomes in the soma (defined by active protease, i.e., red) and for all Alexa Fluor 647-BSA-containing compartments along the length of the major dendrite. Box plots are used to show the 25% and 75% quartile of the data range. The median is indicated. The whiskers show the total data range. $n = 20$ dendrites from two independent experiments were quantified. The number of endosomes quantified is indicated above the graph.

20 cells. Because lysosomes are abundant in the soma, we determined the DQ/Alexa Fluor 647-BSA ratio for 60 somatic DQ-stained compartments (Fig. 5 J). We define these operationally to be degradative lysosomes based on their bright DQ fluorescence. The DQ/Alexa Fluor 647-BSA ratio in different endosomes was highly variable along the dendrite, ranging across more than two orders of magnitude. In the proximal segment, compartments had DQ/Alexa Fluor 647-BSA ratios similar to somatic lysosomes (i.e., highly degradative) as well as >200-fold less DQ/Alexa Fluor 647-BSA intensity values. Some of the compartments thus have little to no degradative capacity. Strikingly, the DQ/Alexa Fluor 647-BSA ratios in more distal compartments showed a smaller range and lower values than the proximal compartments. On average, the ratios were more than ~50-fold lower in the medial (50–75 μm) segments compared with somatic lysosomes. These measurements indicate that the degradative capacity is highly graded along the length of major dendrites. In the more distal segments, a large number of compartments showed very low/no degradative capacity. In agreement with the lower density of many endosomes more distally, we observed fewer BSA-containing compartments with increasing distance from the soma (Fig. 5 J). This experiment thus suggests that degradative capacity was highly heterogeneous in dendrites and was on average about two orders of magnitude higher in the soma and proximal dendrite compared with more distal dendritic segments.

Interference with Rab7 causes accumulation of dendritic cargos in predegradative endosomes along dendrites

Our observations of a steep spatial gradient of degradative capacity along dendrites suggest that dendritic cargos found past the proximal dendritic segment might need to be transported retrogradely to the somatically concentrated lysosomes to degrade. We previously discovered that interference with Rab7 function (either by knockdown of Rab7 or by expression of the dominant-negative [DN] Rab7-T22N [Rab7-DN]) led to accumulation of Nsg proteins in dendritic endosomes (Yap et al., 2017). To test directly whether Rab7-DN led to Nsg accumulation because it prevented degradation, we performed two sets of experiments: we determined whether Rab7-DN led to accumulation of Nsg2 in endosomes (Fig. 6) as well as whether it increased the half-life of Nsg2 (Fig. 7).

As we showed before (Yap et al., 2017), Nsg proteins showed partial colocalization with EEs (Fig. 6 A) and Rab7-GFP (Fig. 6 B, green arrows in B2), including transitioning EEs (EEA1/Rab7-GFP; aqua arrows). When Rab7-DN was expressed (Fig. 6 C), Nsg accumulated to two- to threefold higher levels than GFP or WT Rab7 controls (Fig. 6 B). High accumulation was seen throughout dendrites including in distal endosomes (Fig. 6 C, C3) which corresponded to EEs (blue arrows in line scans; Fig. 6 C, C1 and C2) as well as EEA1⁻ endosomes (red arrows in line scans).

To determine whether Rab7-DN (Fig. 6 E) but not WT Rab7 (Fig. 6 D) also caused Nsg accumulation in LEs along dendrites, we counterstained with LAMP1. Rab7 could not be used as a counterstain because the cytosolic Rab7-DN is also recognized by the antibody. In the proximal dendrite, Nsg accumulated partially with LAMP1 (Fig. 6, E and E'). Similarly, in the juxtaproximal dendrite where LAMP1 is still easily detected, accumulated Nsg

partially colocalized with faint LAMP1 compartments. In contrast, in medial dendrites and beyond, few if any compartments with accumulated Nsg contained LAMP1 (Fig. 6 E'; blue arrows). These observations suggested that Rab7-DN led to accumulation of Nsg distally in predegradative (LAMP1⁻) compartments. We posit that the medial/distal Nsg2-accumulating compartments were early LEs, whereas the proximal ones corresponded to late LEs. In contrast, the abundance, intensity, and localization of LAMP1 itself was not noticeably altered in neurons expressing WT Rab7 or Rab7-DN (Fig. 6, D and E) compared with untransfected neurons in the same field.

Rab7 function is required for terminal degradation of dendritic proteins

Next, we tested whether Rab7-DN expression increased the half-life of Nsg2. Half-lives could not be determined by Western blotting (WB) because of the low transfection efficiency of cultured neurons, and we thus used the IF-based CHX assay (as in Fig. 1 E). Neither expression of GFP (Fig. 7 A) nor WT Rab7-GFP (Fig. 7 B) changed the levels of Nsg2 in untreated controls or after 4 h CHX treatment (green arrows) compared with nontransfected neurons in the same field (aqua arrowheads): Nsg2 degraded similarly and was barely detectable after CHX treatment. In contrast, expression of Rab7-DN-GFP led to accumulation of Nsg2 (green arrows in Fig. 7 C) in untreated controls. Additionally, levels of Nsg2 remained high in the soma and along dendrites even after CHX, whereas nontransfected neighboring neurons had mostly lost Nsg2 staining (aqua arrowheads in Fig. 7 C). DNER behaved similarly and showed accumulation in dendritic endosomes in the presence of Rab7-DN, which persisted even after CHX (Fig. S4). Again, LAMP1 was only occasionally present at low levels at the distal compartments in which Nsg2 accumulated in the presence of Rab7-DN and CHX (Fig. 7, D and E; compare red to purple arrowheads in Fig. 7 D). These Nsg2-containing LAMP1-positive compartments were likely degradation incompetent as Nsg2-accumulating endosomes in the distal dendrites were largely CatB negative (not depicted). Proximally, LAMP1 was often included in the Nsg2-accumulating compartments (Fig. 7 E). In addition, after undergoing endocytosis, Nsg2 failed to degrade in the presence of Rab7-DN (not depicted), consistent with an essential role of Rab7 for the terminal degradation of endocytosed dendritic cargos.

As controls, we expressed DN versions of two additional endosomal Rab proteins, Rab9 and Rab11. Neither Rab is implicated in terminal degradation of cargos. Expression of Rab9-DN-mCherry or Rab11-DN-GFP did not delay degradation of Nsg2 in the presence of CHX (Fig. S5, A–C).

Rab7 function is required for transport of Nsg proteins

Because Rab7-DN caused accumulation of Nsg2 in nondegradative endosomes (Figs. 6 and 7), we hypothesized that Rab7 was required for transport of predegradative dendritic endosomes to the soma to allow subsequent degradation in somatic lysosomes. Because Rab7-DN no longer binds its downstream effectors (Guerra and Bucci, 2016), including adapters for microtubule motors, we wondered whether Rab7 might regulate dendritic motility of Nsg endosomes. We previously showed that Nsg proteins in

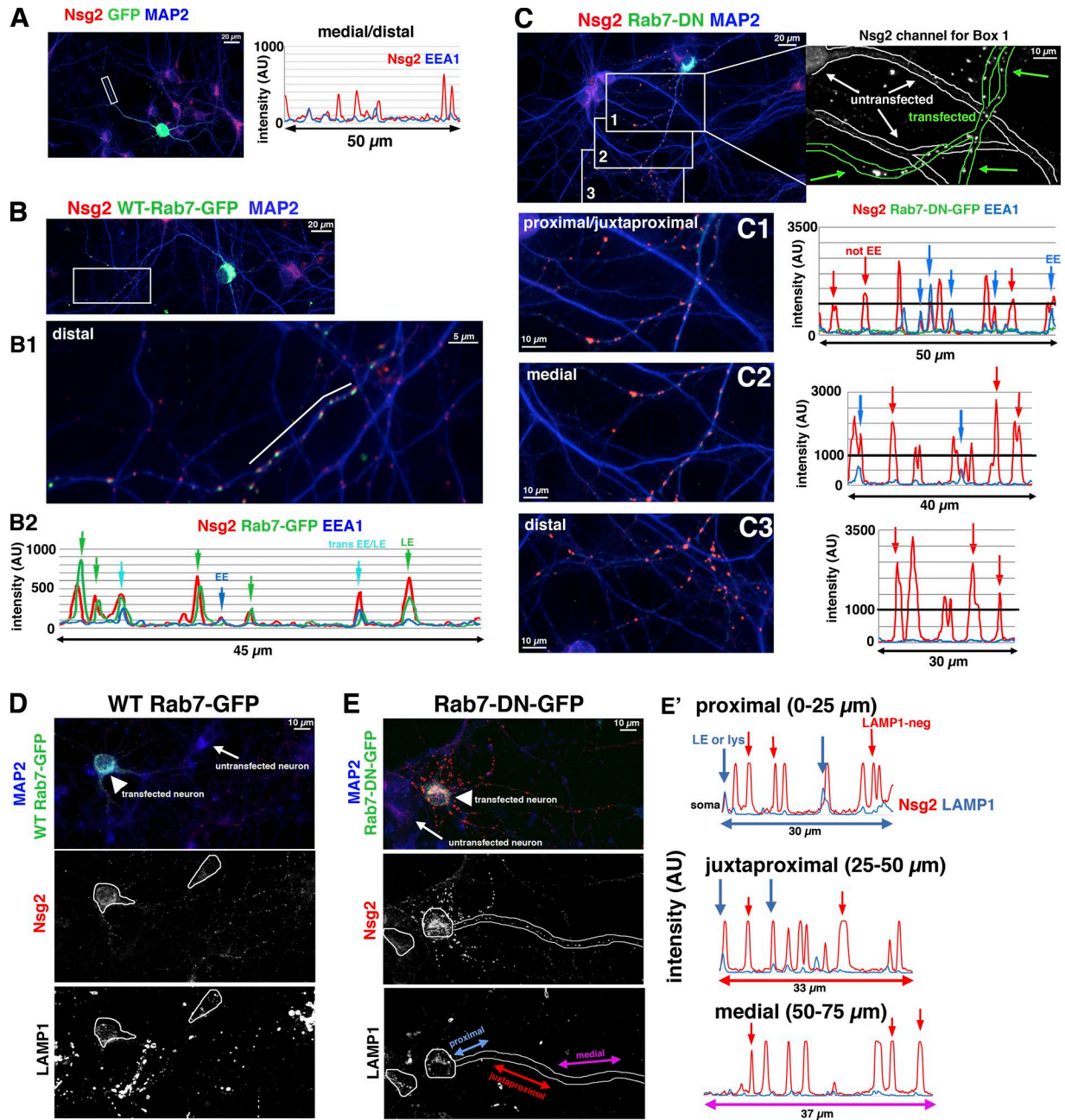


Figure 6. Interference with Rab7 causes accumulation of dendritic cargos in predegradative endosomes along dendrites. (A) Nsg2 (red) is found partially in EEA1-positive (blue) compartments. A line scan of the boxed area shows coinciding peaks. **(B)** When Rab7-GFP is expressed, intensity of Nsg2 peaks is in the same range as for GFP expression, i.e. <1,000 AU (compare line scans in A and B2). Nsg2 along dendrites was found with EEA1 (blue arrow in B2), with Rab7-GFP (green arrows in B2), or in compartments dually positive for EEA1 and Rab7-GFP (aqua arrows in B2). The location of the line scan in B2 is indicated by a white line in B1. B1 corresponds with the boxed region in B. MAP2 (blue) is counterstained to identify dendrites. **(C)** Neurons expressing Rab7-DN-GFP show accumulation of endogenous Nsg2 (red) along dendrites (marked with MAP2 in blue). The proximal (C1), medial (C2), and distal (C3) dendritic regions (boxes in C) are shown with corresponding line scans. Note the different scale on the Y axis compared with B2. The Nsg2 channel alone corresponding with C1 is shown on the right of C to allow comparison of Nsg2 staining intensities in Rab7-DN-GFP-expressing dendrites (outlined in green) with nontransfected dendrites (outlined in white). Nsg2 accumulates in EEA1-positive EEs (blue arrows) and in EEA1-negative compartments (red arrows). Images are representative of five independent repeats. **(D and E)** Cells expressing WT Rab7-GFP (D) or Rab7-DN-GFP (E) were counterstained with MAP2 (blue), Nsg2, and LAMP1. Single channels are shown below. Line scans along the double-headed color-coded arrows in E are shown in E'. Nsg2 (red) accumulates partially in LAMP1-positive compartments (blue arrows in E') but more frequently in LAMP1-negative compartments (red arrows in E'). LAMP1 levels were not changed in WT Rab7-GFP-expressing neurons (D; white arrowhead) or in Rab7-DN-GFP-expressing cells (E; white arrowhead) compared with untransfected neurons. Cell bodies are encircled for easier comparison.

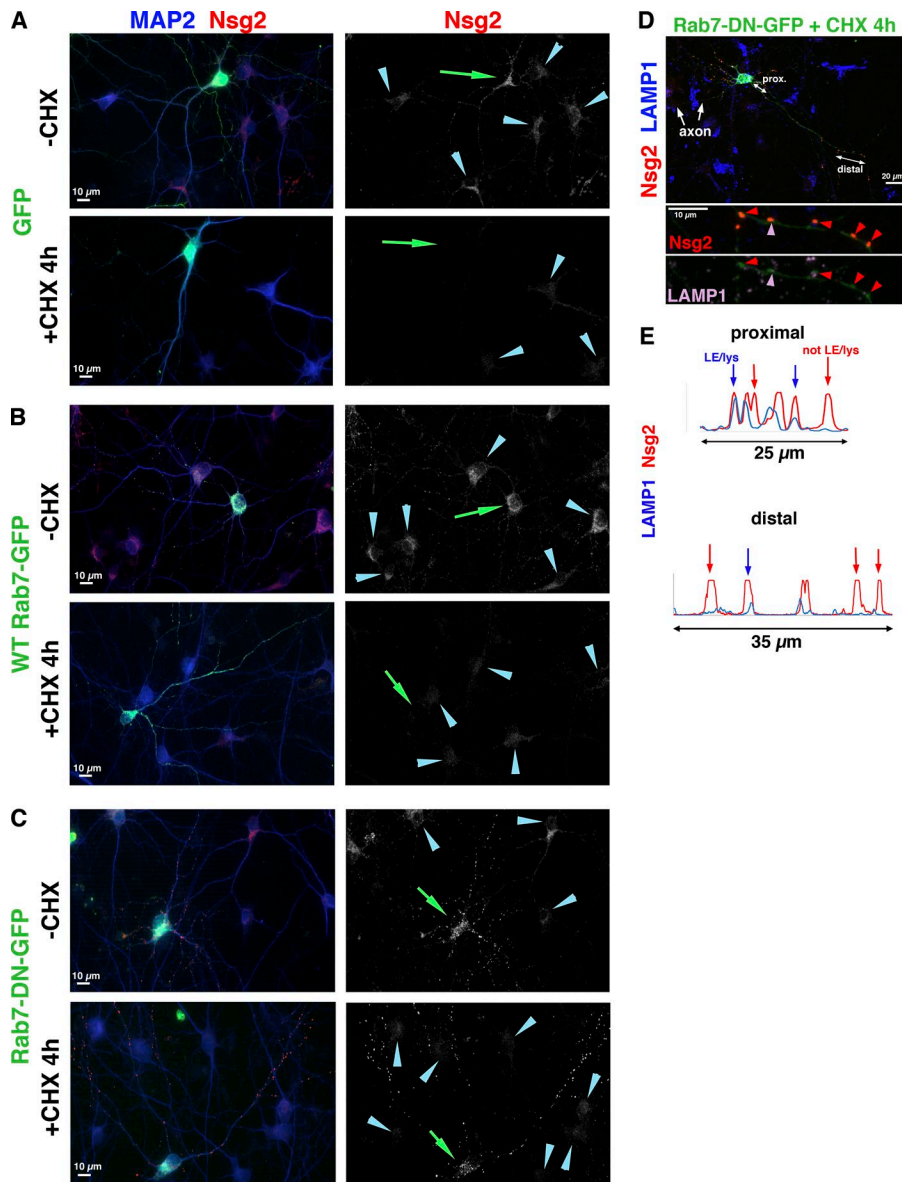


Figure 7. Rab7 function is required for terminal degradation of dendritic proteins. (A–C) Neurons were transfected with GFP (A), WT Rab7-GFP (B), or Rab7-DN-GFP (C) and either treated with CHX for 4 h (+CHX 4h) or not treated (-CHX). Nsg2 (red) single-channel images are shown on the right. Nsg2 levels were greatly diminished after 4 h CHX in GFP- (A) and WT Rab7-GFP- (B) expressing neurons, but Nsg2 persisted when Rab7-DN-GFP (C) was expressed. Green arrows indicate untransfected cells. Aqua arrows indicate untransfected cells. MAP2 (blue) marks dendrites. Images are representative from one experiment (out of a total of five independent repeats). **(D and E)** LAMP1 counterstain of a CHX-treated Rab7-DN-GFP-expressing neuron after 4 h chase. The bottom panel reveals low colocalization of accumulated Nsg2 (red arrowheads), with LAMP1 (purple arrowheads) in distal dendrites. The regions of close up indicated by double-headed arrows (“prox.” and “distal”) on the top are shown as line scans in E (blue arrows indicate LAMP1-positive compartments; red arrows indicate LAMP1-negative compartments).

dendrites frequently move together with Rab7 (Yap et al., 2017). We thus determined by live imaging whether expression of Rab7-DN impeded the motility of endosomes containing Nsg1-mCherry. GFP and WT Rab7-GFP were expressed as controls. Nsg1-mCherry-positive carriers were frequently motile in controls but were mostly stationary in Rab7-DN-expressing neurons, with only short bidirectional excursions (Fig. 8, A and B). To determine whether the motility of other cargos was also slowed by expression of Rab7-DN, we performed live imaging of LAMP1-RFP (Fig. 8, C and D) and of transferrin receptor (TfR)-cherry (Fig. 8, E and F), which is transported in recycling endosomes. No differences of LAMP1-RFP or TfR-cherry motility were found between WT Rab7 and Rab7-DN (Fig. 8, C–F). It was surprising to find no effect on LAMP1 motility because Rab7 at least partially colocalized with LAMP1 (see Fig. 3 E). Interference with Rab7 function thus preferentially interfered with transport of cargos fated for degradation.

When live imaging of Nsg1 was performed in neurons expressing Rab9-DN or Rab11-DN, no apparent changes in Nsg1

motility were observed compared with GFP (Fig. S5, D–F). Our data are consistent with the model that the lack of degradation of Nsg proteins in Rab7-DN is a result of lack of transport of more distally located compartments to the more centrally localized lysosomes. It is likely that additional Rab7-regulated steps such as fusion with lysosomes, which needs to take place downstream of transport for degradation to occur, would also be impaired by expression of Rab7-DN.

Inhibition of lysosomal proteases leads to preferential accumulation of Nsg proteins in somatic and not dendritic endosomes

Because Rab7-DN caused both accumulation and impaired motility of Nsg2 along dendrites, we posited that Rab7 is required for transport of predegradative endosomes to degradative lysosomes in the soma. We thus wondered whether if we inhibited degradation directly (using Leu) but not transport, would we see accumulation only in somatic compartments but not along

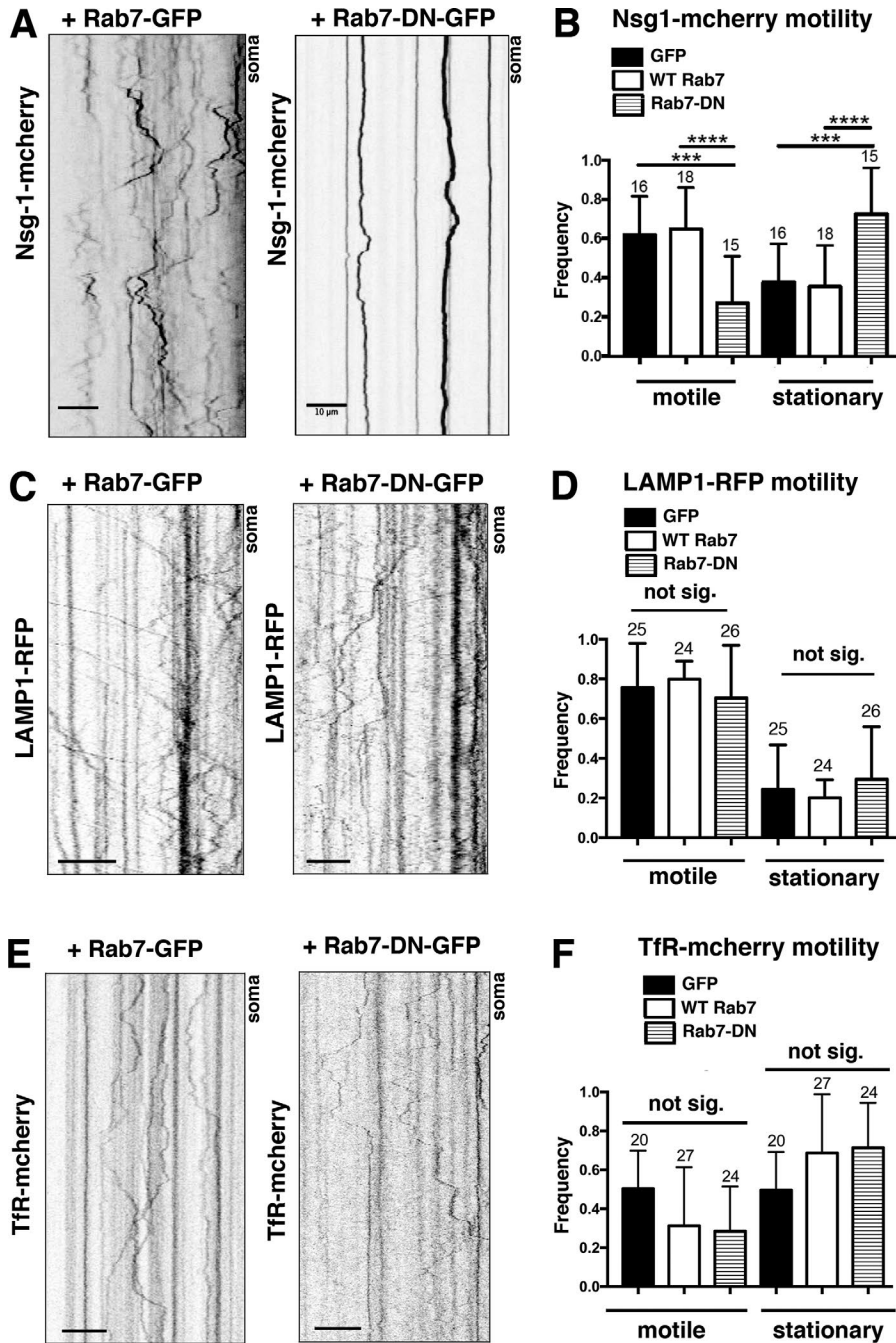


Figure 8. Interference with Rab7 leads to decreased motility of Nsg proteins but not of TfR or LAMP1. (A and B) The motility of Nsg1-mCherry was significantly inhibited in cells expressing Rab7-DN-GFP compared with GFP or WT Rab7-GFP. Examples of kymographs (500 s) are shown in A (soma on the right), and quantifications are in B. (C–F) No statistically significant changes in the motility of the nondegradative cargos LAMP1-RFP (C and D) or TfR-mCherry (E and F) were observed. Numbers above the bars are numbers of cells (from three independent cultures). For each cell, counts from all dendrites were averaged to derive a single number per cell. Total dendrite numbers were 52–62 for Nsg1 videos, 110–140 for TfR videos, and 79–108 for LAMP1 videos. One-way ANOVA (Nsg1) or Kruskal-Wallis (TfR and LAMP1) tests were used. ***, $P < 0.0003$; ****, $P < 0.0001$.

dendrites. We first tested the effects of Leu on protein half-life (Fig. 9 A). Alternatively, cultures were treated with CHX for 20 h. Long-lived membrane proteins showed moderate changes in protein levels when new synthesis was inhibited with CHX for 20 h (quantification of blot: GluA2, >52%; L1, >42%; syntaxin13, >59%; and syntaxin7, >75%). When lysosomal degradation was inhibited with Leu for 20 h, no significant accumulation occurred for these proteins (80–100% remaining). In contrast, Nsg proteins were undetectable after 20 h CHX treatment, and their levels increased 1.7- to twofold after Leu treatment, demonstrating that their steady-state levels are tightly regulated by new synthesis and lysosomal degradation. Interestingly, the levels of cathepsins were largely unaffected by CHX treatment but were increased

(~150% of control) after Leu treatment. A second slower-mobility band could be detected in Leu, which likely corresponds with uncleaved pro-forms of cathepsins (Fig. 9 A). By IF, we observed a significant increase in somatic Nsg protein staining after Leu treatment of neurons (Fig. 9, B and C) but no increase in somatic Rab7 or EEA1 staining (Fig. 9 C), supporting our hypothesis that somatic lysosomes were responsible to a large extent for the terminal degradation of these short-lived proteins.

Nsg2 is endocytosed along dendrites and in the soma and disappears from both soma and dendrites almost completely when chased for 4 h (Yap et al., 2017). We reasoned that if we performed the Nsg2 endocytosis and subsequent chase assay in the presence of Leu, endocytosed Nsg2 would accumulate in those

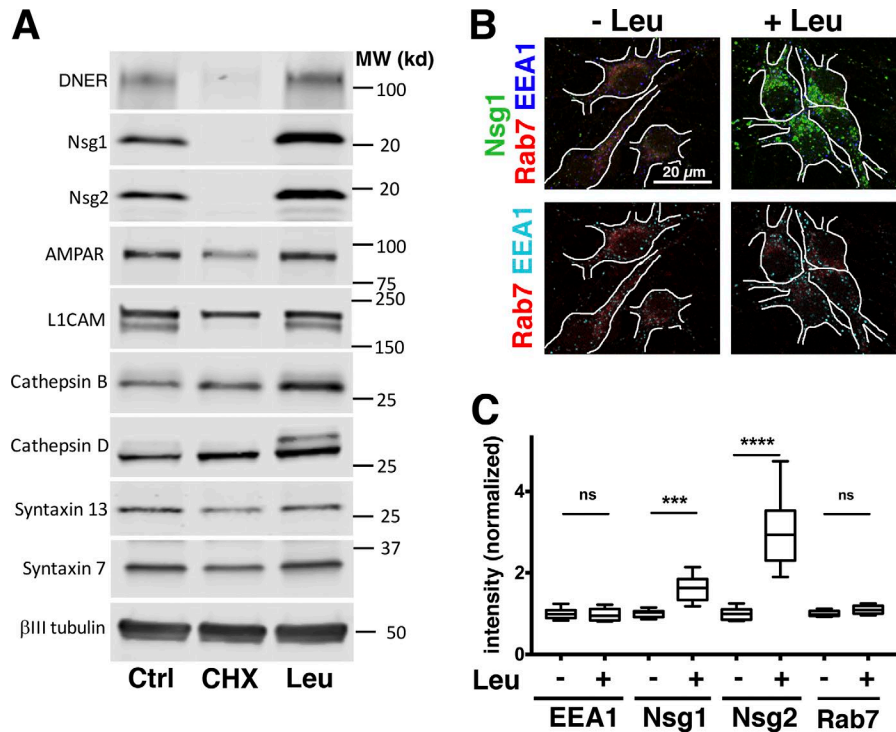


Figure 9. The steady-state levels of Nsg1, Nsg2, and DNER are highly sensitive to inhibitors of protein synthesis or lysosomal proteases. (A) Levels of proteins in neuronal cultures revealed by WB after 20 h CHX or Leu treatment. MW, molecular weight. (B) Immunostaining of neuronal cultures against endogenous Nsg1 (green), Rab7 (red), and EEA1 (blue) after treatment for 20 h with and without Leu. The experiment was performed in at least five independent cultures, and representative images from one experiment are shown. (C) Quantification of EEA1, Nsg1, Nsg2, and Rab7 levels in somatic endosomes. $n = 10$ fields (6–10 neurons per field) from two independent experiments were quantified and normalized to - Leu levels. Box plots are used to show the median and 25% and 75% quartiles. The whiskers show the full range of the data. The data passed a normality test, and a t test was used to compare with and without Leu for each marker. ***, $P < 0.0003$; ****, $P < 0.0001$.

compartments where the bulk degradation would normally take place in the absence of Leu. This assay would thus allow us to quantify the extent of dendritic versus somatic bulk degradation. If the endocytosed Nsg2 was significantly degraded locally in dendritic lysosomes, we should observe accumulation of nondegraded endocytosed Nsg2 along dendrites after the chase. In controls without Leu, endocytosed Nsg2 was abundantly present in both the soma and dendrites (Fig. 10 A). After 4 h chase, no endocytosed Nsg2 remained in either soma or dendrites (Fig. 10 B). When Leu was included in the experiment, endocytosis of Nsg2 was similar to controls without Leu (Fig. 10 C), but substantial accumulation of endocytosed Nsg2 was observed after 4 h chase (Fig. 10 D). In the soma, Leu completely blocked the decrease of Nsg2 intensity (Fig. 10 E). In contrast, Leu did not block the decrease of Nsg2 intensity that occurred in dendrites (Fig. 10 F). We thus propose that terminal degradation of Nsg2 mostly occurs in somatic lysosomes and not along dendrites.

Discussion

Our recent discovery of the very short half-lives of the somatodendritic endosomal Nsg proteins prompted us to determine where in neurons their terminal degradation took place and how it was regulated (Yap et al., 2017). We demonstrate in this study that the majority of dendritic LAMP1⁺ endosomes are not degradative lysosomes and that terminal degradation of dendritic cargos such as Nsg1 and Nsg2 requires retrograde Rab7-dependent transport to somatic degradative lysosomes. The same pathway operates for another short-lived dendritic receptor, DNER. DNER is important in cerebellar development, but its exact roles are not well established (Eiraku et al., 2005). In addition, we discovered that medial and distal dendrites have abundant populations of Rab7-positive/LAMP1-negative/LysoTracker-negative

endosomes that were not previously described in dendrites. We are calling these endosomes early LEs and posit that they are maturing LEs transporting to-be-degraded cargos to the soma. These observations raise important questions about how overall protein homeostasis is regulated in distal portions of dendrites, which largely lack degradative lysosomes.

Defining distinct endosomal compartments along dendrites: Using multiple markers against endogenous proteins

The question of where lysosomes are located in neurons is surprisingly controversial. Several laboratories reported over many years that lysosomes (defined by LAMP1) tend to cluster in the neuronal soma (Cai et al., 2010; Maday and Holzbaur, 2016). Older work concluded that LEs (Rab7) as well as lysosomes (LAMP1 or endocytosed HRP) were clustered in the soma (Parton et al., 1992). Other work, in contrast, has described abundant lysosomes in axons and dendrites (Lee et al., 2011; Schwenk et al., 2014; Farías et al., 2017), using many of the same markers. Furthermore, Ehlers (2000) showed that AMPAR entered LAMP1-positive endosomes in dendrites and degraded rapidly after activity, but whether degradation took place locally was not clear. Along the same lines, recent work from several laboratories not only showed lysosomes in dendrites (Farías et al., 2017) but demonstrated activity-dependent transport of lysosomes to dendritic spines (Goo et al., 2017) or local secretion of CatB at spines triggered by back-propagating action potentials (Padamsey et al., 2017).

These apparently contradictory findings are caused in part by different definitions of what constitutes a lysosome. For instance, Rab7 and LAMPs are frequently interchangeably used to denote lysosomes (Schwenk et al., 2014). Similarly, LEs and lysosomes are often combined into a single category, and overexpressed markers (especially LAMP1-GFP) are used as stand

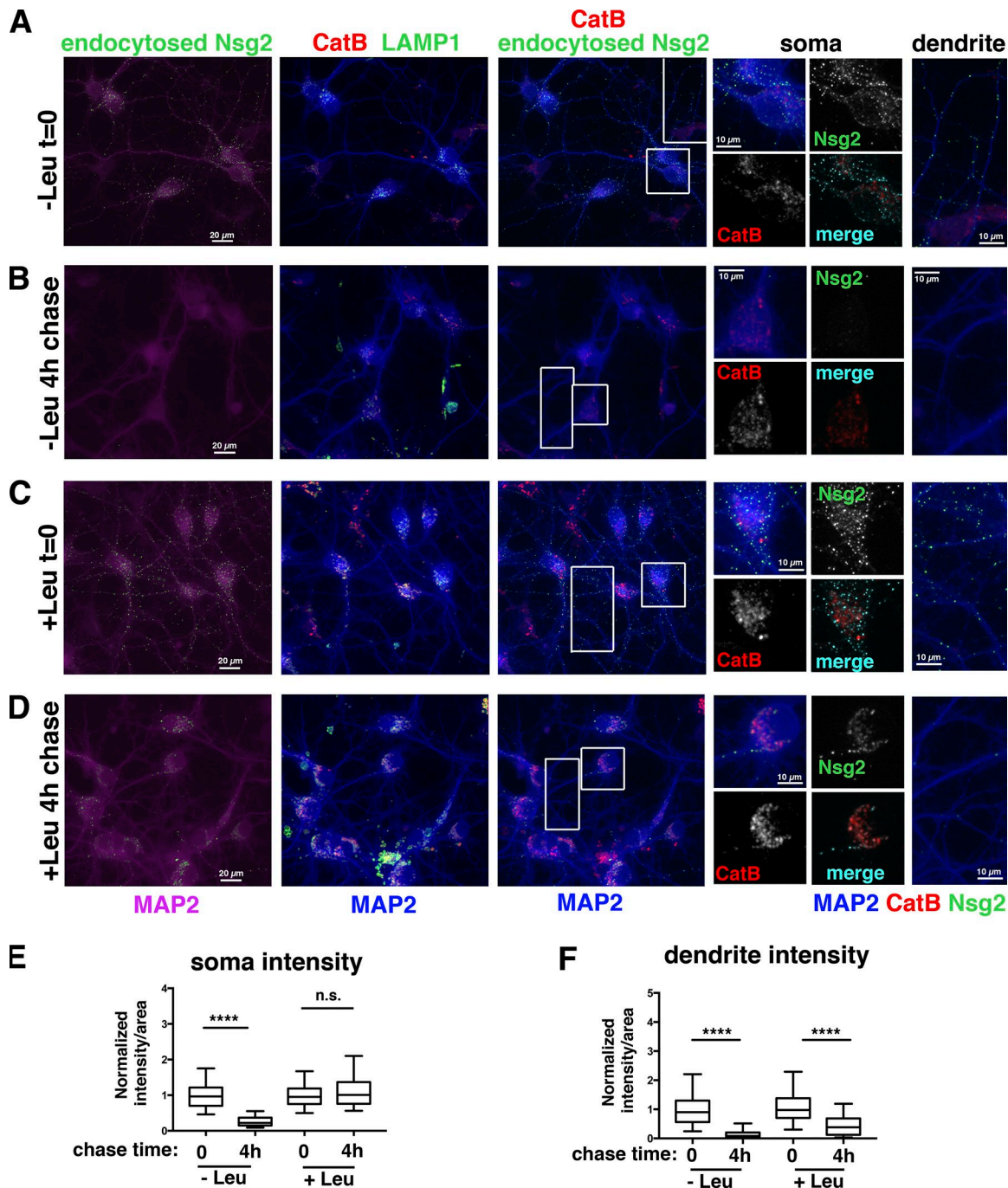


Figure 10. **Inhibition of lysosomal proteases leads to preferential accumulation of Nsg proteins in somatic and not dendritic endosomes.** (A–D) DIV 9 neurons were incubated without (A and B) or with Leu (C and D), and an endocytosis assay against endogenous Nsg2 was performed. Cells were either fixed directly after antibody loading ($t = 0$; A and C) or endocytosed antibody was chased for 4 h ($t = 4$ h; B and D). MAP2 is shown in combination with endocytosed Nsg2, LAMP1, or CatB as indicated. Close ups of the soma and dendrites are shown on the right. The positions of the close ups are indicated by the white boxes (soma) and white rectangles (dendrites). A slight increase of the intensity of CatB in neurons treated with Leu was observed. (E and F) The fluorescence intensity of endocytosed Nsg2 in the soma (E) or along dendrites (F) was quantified. Box plots are used to show the median and 25% and 75% quartiles. The whiskers show the fifth to 95th percentiles of the data range. $n = 160$ – 300 cells per condition. Two representative experiments were quantified (from a total of four independent cultures). A Kruskal-Wallis test was used. ****, $P < 0.0001$.

ins for revealing LE/lysosome localization (Farías et al., 2017). For our purposes of identifying where degradative capacity is localized in dendrites, we defined lysosomes as acidified LAMP1-positive compartments containing active cathepsins. We made use of a multitude of markers and determined the distribution of

endogenous proteins, most often as combinations of three endogenous endosomal proteins simultaneously. In addition, we determined how distribution of endosomal subpopulations changed with distance from the soma along dendrites. This has not been done quantitatively before and led to our discovery of a spatial

gradient of endosomal populations along dendrites as well as to the identification of subpopulations of endosomes not previously described in dendrites, namely Rab7-positive/LAMP1-negative early LEs and LAMP1-positive/Rab7-negative compartments of unknown function (Fig. 4, C and D).

A model for endosome maturation along dendrites

We find that (EEA1 positive) EEs and (Rab7 positive) LEs are widely distributed throughout soma and dendritic arbors. This agrees with our previous data showing that dendritic EEs largely do not move in dendrites and convert to LEs locally (Lasiecka et al., 2014; Yap et al., 2017). LEs (Rab7 positive), however, have substantial motile populations in dendrites (Schwenk et al., 2014; Yap et al., 2017). We propose that LEs (Rab7 positive) in medial and distal dendrites are the major retrograde carrier for bulk degradative cargos back to the soma. Degradative lysosomes (CatB/D positive/LAMP1 positive), in contrast, are mostly present in the soma and proximal portion of the major dendrites and almost never found in the minor dendrites (Fig. 4 D). Other lysosomal hydrolases might be found more distally, and certain substrates might be cleaved there, but this remains to be shown. Interestingly, axon terminals in *Drosophila melanogaster* have distinct degradative local machinery for synaptic vesicle proteins (Jin et al., 2018).

Interestingly, unique LAMP carriers have been identified in fibroblasts that deliver LAMP to LEs separately from cathepsins (Pols et al., 2013). Given the large extent of neuronal arbors and our discovery of steep spatial gradients of endosomal subpopulation in dendrites, where and how LAMPs and cathepsins are delivered to LEs/lysosomes in dendrites is an open question. Furthermore, lysosome-related organelles containing low hydrolase activity are present in axons and accumulate in Alzheimer's disease (Lee et al., 2011; Gowrishankar et al., 2015, 2017). Unlike our findings in dendrites, however, Rab7 and LAMP1 are acquired more or less at the same time in distal axons (Lee et al., 2011). Similarly to our findings in dendrites, Rab7-positive/LAMP1-positive LEs in axons subsequently acquire CatB as they near the soma (Lee et al., 2011).

Rab7 is required for transport and terminal degradation of dendritic proteins

Our data support the conclusion that terminal degradation of dendritic cargos requires Rab7-dependent transport. Rab7 is implicated in multiple steps of endosomal progression including the conversion of EEs to LEs (Liu et al., 2017), transport of LEs, and fusion of LEs with lysosomes (Vanlandingham and Ceresa, 2009; Huotari and Helenius, 2011). Active Rab7 has a multitude of effectors that regulate recruitment of microtubule motors, recruitment of tethering complexes for subsequent fusion, recruitment of retromer complex for transport to the trans-Golgi network, and acidification (Wang et al., 2011; Guerra and Bucci, 2016). Rab7-DN is incapable of binding to any of its downstream effectors, and its expression thus causes cessation of transport as well as disruption of LE/lysosome fusion and acidification in fibroblasts (De Luca et al., 2014). Analogously to other cell types, overexpression of Rab7-DN in neurons resulted in a decrease in the movement of Nsg endosomes and accumulation of Nsg/

DNER endosomes along dendrites after CHX treatment. These effects are presumably caused by loss of motor recruitment to endosomes, but the detailed underlying molecular mechanisms will require additional study. We propose that terminal degradation of these short-lived dendritic membrane proteins occurs in somatic lysosomes after retrograde transport in dispersed Rab7-positive predegradative LEs in dendrites. In fibroblasts, peripheral LAMP1 compartments were also found to be less acidic (Johnson et al., 2016), possibly providing an analogous example.

Interestingly, interference with Rab7 function leads to defects in dendrite maintenance in cultured neurons (Schwenk et al., 2014). Additionally, delayed dendrite growth was observed in the absence of the newly discovered Rab7 effector WDR91 (Liu et al., 2017), highlighting the physiological importance of Rab7 effector function and endosome maturation in dendrite maintenance. These dendritic phenotypes could be caused by either disturbance of growth factor signaling from endosomes or by changes in bulk degradation or both (Casanova and Winckler, 2017). In addition, Rab7 function is required for long-term depression (Kim et al., 2017), likely by biasing glutamate receptors from recycling toward degradation (Fernández-Monreal et al., 2012).

Rab7 also plays an important role in axons (Guerra and Bucci, 2016; Ponomareva et al., 2016). This is significant as mutations in Rab7 are genetically linked to Charcot-Marie Tooth disease 2B, a genetic disorder resulting in axonal neuropathy in the peripheral nervous system (Cogli et al., 2009). The axonal pathology might be caused by altered nerve growth factor signaling from Rab7-containing TrkA signaling endosomes (Liu and Wu, 2017). Additional pathways are also regulated by Rab7 in axons (Cherry et al., 2013; Ponomareva et al., 2016), likely by affecting the half-lives of additional cargos other than TrkA. Similarly, the final positioning of migratory neurons is regulated by Rab7 early in cortical development (Kawauchi et al., 2010), and N-cadherin is one of the proposed cargos regulated by Rab7 during neuronal migration.

In conclusion, we show that terminal degradation of dendritic membrane proteins overwhelmingly takes place in the soma or proximal dendrite. Because protein homeostasis needs to be maintained for neuronal health and is frequently at the center of neurodegenerative pathologies (Douglas and Dillin, 2010), it will be important to take the spatial distribution of degradative potential into account.

Materials and methods

Antibodies

Anti-Nsg1 antibody using the same peptide sequences against the N terminus of Nsg1 from aa 7 to 23 (NFAEKGTKQPLEDGF) as in Steiner et al. (2002) was raised in rabbits by Thermo Fisher Scientific and in goats by Everest Biotech with peptide sequences from aa 7 to 20 (1:300 IF; EB11637; RRID: AB_2554545; Yap et al., 2017).

Lists of other antibodies used in this study: anti-Nsg2 (rabbit monoclonal; 1:500 IF; ab18953; RRID: AB_2571866; Abcam), anti-Nsg2 (goat polyclonal; 1:400 IF; EB12967; Everest Biotech), anti-L1CAM (clone 2C2; mouse monoclonal; 1:1,000 WB; ab24345; RRID: AB_448025; Abcam), anti-AMPA2 (GluR2;

clone 6C4; mouse monoclonal; 1:200 IF; 1:1,000 WB; MAB397; RRID: AB_11212990; EMD Millipore), anti-GluR1 (clone D4N9V; rabbit monoclonal; 1:200 IF; 13185; Cell Signaling Technology), anti-syntaxin13 (rabbit polyclonal; 1:1,000 WB; 110-133; Synaptic Systems), anti-syntaxin7 (sheep polyclonal; 1:1,000 WB; AF5478; RRID: AB_2239977; R&D Systems), anti-CatB (goat polyclonal; 1:500 IF; 1:100 immunohistochemistry; 1:1,000 WB; AF965; RRID: AB_2086949; R&D Systems), anti-CatD (goat polyclonal; 1:500 IF; 1:1,000 WB; AF1029; RRID: AB_2087094; R&D Systems), anti-DNER (goat polyclonal; 1:500 IF; 1:1,000 WB; AF2254; RRID: AB_355202; R&D Systems), anti-LAMP2 (rat monoclonal; 1:1,000 WB; ABL-93; RRID: AB_2134767; Developmental Studies Hybridoma Bank), anti-LAMP1 (clone 1D4B; rat monoclonal; 1:100 immunohistochemistry; 1D4B; RRID: AB_2134500; Developmental Studies Hybridoma Bank), anti-EEA1 (mouse monoclonal; 1:100 IF; 1:1,000 WB; 610456; RRID: AB_399409; BD), anti-LAMP1 (mouse monoclonal; 1:2,000 IF; ADI-VAM-EN001; RRID: AB_2038958; Enzo Life Sciences), anti-MAP2 (chicken polyclonal; 1:2,000 IF; CPCA-MAP2; RRID: AB_2138173; EnCor Biotechnology), and anti- β III tubulin (chicken polyclonal; 1:7,500 WB; TUJ; Aves Lab). For Rab7 staining, anti-Rab7 (rabbit monoclonal; 1:100 IF; 1:1,000 WB; 9367; RRID: AB_1904103) was used. The specificity of this Rab7 antibody was validated previously (Ding et al., 2017), and its specificity confirmed by us in neurons using shRNA against Rab7 (Fig. S1).

Secondary antibodies

Alexa Fluor-coupled antibodies (Thermo Fisher Scientific and Molecular Probes): Alexa Fluor 488 donkey anti-mouse (A21202), Alexa Fluor 488 donkey anti-rabbit (A21206), Alexa Fluor 488 donkey anti-goat (A11055), Alexa Fluor 568 donkey anti-mouse (A10037), Alexa Fluor 568 donkey anti-rabbit (A10042), Alexa Fluor 568 donkey anti-goat (A11057), Alexa Fluor 647 donkey anti-mouse (A31571), Alexa Fluor 647 donkey anti-rabbit (A31573), Alexa Fluor 647 donkey anti-goat (A21447); Jackson ImmunoResearch Laboratories, Inc., antibodies: aminomethylcoumarin donkey anti-chicken (703-155-155) and rhodamine red-X donkey anti-rat (712-295-153). For LI-COR Biosciences Odyssey WBs, Jackson ImmunoResearch Laboratories, Inc., donkey anti-mouse (680; 715-625-151), donkey anti-rabbit (790; 711-655-152), donkey anti-sheep (680; 713-625-147), donkey anti-rat (680; 712-625-153), and donkey anti-goat (800; 926-32214; LI-COR Biosciences) antibodies were used.

Plasmids

Nsg1-Emerald was from Addgene (54202; from M. Davidson, Florida State University, Tallahassee, FL); the mutation at residue 114 from D to G was corrected. For *Nsg1-mCherry*, WT mouse *Nsg1* was cloned into pmCherry-N1 (Takara Bio Inc.). Rab7-GFP (12605) and Rab7-DN(T22N)-GFP (12660) were from Addgene (R. Pagano, Mayo Clinic, Rochester, MN). *mTagBFP2-Rab7* was from M. Davidson. Lamp1-mRFP-Flag was from Addgene (34611; from D. Sabatini, Massachusetts Institute of Technology, Cambridge, MA). GFP-Rab11DN(S25N) was from I. Mellman (Genentech, South San Francisco, CA). mCherry-Rab9DN(S21N) was a gift from J. Casanova (University of Virginia, Charlottesville, VA); a human Rab9DN was cloned into pmCherry vector. GFP

was from Takara Bio Inc. mCherry-TFR-20 was from Addgene (55144; from M. Davidson). shRNA plasmids against the rat Rab7a were obtained from QIAGEN's SureSilencing (KR42489G). The shRNAs were expressed under the control of the U1 promoter and contained a GFP reporter gene. The sequence of the shRNA 2 was: 5'-CAGCTGGAGAGACGAGTTTCT-3'. The scrambled sequence used as control (shRandom) was 5'-GGAATCTCATTCGATGCATAC-3'.

Neuronal cultures and transfections

Neuronal cultures were prepared from E18 rat hippocampi as described by Yap et al. (2017). All experiments were performed in accordance with Institutional Animal Care and Use Committee guidelines and regulations. Hippocampi from all pups in one litter were combined and thus contained male and female animals. Cells were plated on poly-L-lysine-coated coverslips and incubated with plating medium containing DMEM with 10% horse serum. For live-imaging use, neurons were plated on a 35-mm glass-bottomed microwell dish (MatTek). After 4 h, the plating medium was removed and replaced with serum-free medium supplemented with B27 (Thermo Fisher Scientific), and neurons were cultured for 7–10 DIV for experimental use. Transfections were performed with Lipofectamine 2000 (Invitrogen). Neurons (DIV 7–8) were transfected with either GFP, Rab7-GFP, Rab7-DN-GFP, Rab9-DN, or Rab11-DN for 36–40 h and then treated with/without cycloheximide (CHX) (20 μ g/ml) for 4 h. To investigate the effect of degradation inhibition on neuronal-specific membrane proteins, neurons were treated with Leu (20 μ M; Sigma-Aldrich) for 20 h. All transfection and inhibitor treatment experiments were repeated in 5–10 independently derived cultures. Experiments investigating endogenous proteins localization (*Nsg1*, *Nsg2*, *DNER*, *Rab7*, *EEA1*, *CatB*, and *LAMP1*) were repeated in at least three independent cultures and quantified from at least two of them.

Immunocytochemistry, endocytosis assay, and image acquisition

All immunocytochemistry, endocytosis assay, and image acquisition were done as described by Yap et al. (2017). In brief, cells were fixed in 2% paraformaldehyde/3% sucrose/PBS in 50% conditioned medium at room temperature for 20 min and then quenched in 10 mM glycine/PBS for 10 min. Coverslips were then blocked in 5% horse serum/1% BSA/PBS + 0.2% Triton X-100 or 0.1% saponin for 20 min. Antibodies were diluted in 1% BSA/PBS and incubated for 1 h at room temperature. Coverslips were mounted in ProLong Gold mounting medium (P36930; Thermo Fisher Scientific).

Endocytosis assay

Neurons (DIV 8–10) were incubated with anti-DNER or anti-Nsg2 antibodies for 30 min at 37°C. To remove surface-bound antibody without damaging the cells, we washed neurons with PBS twice, followed by a 1-min treatment with DMEM, pH 4.0, followed by two more PBS washes before returning to the incubator for various time points. To ensure no remaining surface-bound antibody that might be misinterpreted as internalized antibody, neurons were washed once with MEM, pH 2.0, for 30 s before fixation

in 2% paraformaldehyde/3% sucrose/PBS, pH 7.4. Internalized antibody was detected by applying secondary antibodies after permeabilization. For endocytosis assays in neurons treated with Leu, we treated DIV 8 neurons with/without 20 μ M of Leu for 20 h, followed by endocytosis of anti-Nsg2, and then chased the endocytosed antibody in the presence/absence of Leu for the indicated time. Endocytosis assay experiments were repeated in at least three independently derived cultures (see figure legends for number of repeats for each experiment). If phenotypes were consistently observed, rigorous quantification was performed in two representative experiments of the total experiments.

Image acquisition

All fixed samples were viewed on an AxioObserver.Z1 with a 40 \times objective (enhanced chemiluminescence Plan-Neofluor 40 \times /0.9 Pol; working distance, 0.41; ZEISS). Apotome.2 structured illumination was used for most images. Images were captured with the AxioCam 503 camera using Zen software (2012 blue edition; ZEISS) and processed identically in Photoshop (Adobe). No non-linear image adjustments were performed. For quantification of colocalization and protein abundance, z stack images of fixed samples were acquired using a 40 \times oil objective (LD-C Apochromat; 1.3 NA) with a 1-AU pinhole on an inverted LSM880 laser scanning confocal microscope (ZEISS). Two tracks of laser lines were used to capture images of four channels: 405 nm/568 nm and 488 nm/647 nm. On average, 10–20 fields were captured per experiment. All images and line scans are representative examples that are highly reproducible and robust.

Immunohistochemistry

Mice (Thy1-GFP M line) were maintained on a 12-h light/dark cycle and allowed ad libitum access to food and water. Experiments were conducted according to protocols approved by Drexel University Institute for Animal Care and Use Committee and Research Animal Resource Center. Animals were given an intraperitoneal injection of ketamine/xylazine/acepromazine and were transcardially perfused with 20–30 ml of PBS followed by 60 ml of 4% paraformaldehyde. Brains were dissected and post-fixed for 2–4 h followed by cryoprotection in 30% sucrose and then were stored at 4 $^{\circ}$ C until ready for sectioning. Tissue was sectioned on a cryostat at 40 μ m, and serial sections were collected in 96-well plates containing 0.05% sodium azide and then stored at 4 $^{\circ}$ C until ready for immunostaining. Tissue sections were processed as described by Barford et al. (2017) except that the antigen retrieval step was omitted. In brief, sections were rinsed three times with 1 \times PBS and incubated with blocking solution (0.2% Triton X-100 and 3% normal donkey serum) for 1 h at room temperature. Sections were then incubated with primary antibodies diluted in blocking buffer overnight at 4 $^{\circ}$ C. The next day, sections were washed with 1 \times PBS three times and incubated with secondary antibodies for 1 h at room temperature protected from light. Finally, sections were incubated with DAPI (D1306; Thermo Fisher Scientific) for 10 min at room temperature followed by 3 \times washing with 1 \times PBS, and then they were mounted with ProLong diamond antifade mounting media (P36970; Thermo Fisher Scientific). Z stack images of fixed brain sections were acquired using a 40 \times oil objective (LD-C Apochromat; 1.3 NA) with 1-AU

pinhole on an inverted LSM880 laser scanning confocal microscope. Two tracks of laser lines were used to capture images of four channels: 405 nm/568 nm and 488 nm/647 nm.

Functional labeling of lysosomes

LysoTracker dyes [LysoTracker Red [DND-99; 1:10,000 \times L7528; Thermo Fisher Scientific] or LysoTracker Green [DND-26; 1:10,000 \times ; 8783P; Cell Signaling Technology]] were used to live label and track acidified compartments in transfected neurons using the manufacturer's protocol. We used MR-Cat assay kits (1:1,300 dilution; 937, 939, and 941; Immunochemistry Technologies) to live label active CatB, K, and L in transfected neurons according to the manufacturer's protocol. DIV 8 GFP-transfected neuronal cultures were incubated with 25 μ g/ml DQ-BSA (DQ-BSA red; D12051; Thermo Fisher Scientific) and 25 μ g/ml BSA-Alexa Fluor 647 (BSA-Alexa Fluor 647 conjugate; A34785; Thermo Fisher Scientific) at 37 $^{\circ}$ C for 2 h to live label protease-mediated hydrolysis of BSA together with endocytosed BSA-Alexa Fluor 647 compartments. BSA-Alexa Fluor 647 is fluorescent regardless of pH and does not require proteolysis for fluorescence. It was thus used to label all endosomes. To investigate the effect of degradation inhibition on DQ-BSA labeling, DIV 9 neurons were preincubated with 200 μ M Leu for 2 h followed by another 2 h incubation with 50 μ g/ml of DQ-BSA in the presence of Leu. Images were captured live with the AxioCam 503 camera on the AxioObserver.Z1 with a 40 \times objective (enhanced chemiluminescence Plan Neofluor 40 \times /0.9 Pol; working distance, 0.41) using Zen software and processed identically in Photoshop. Imaging of live labeling of lysosomal markers in neurons was repeated in at least three independent cultures.

Live imaging and kymograph analysis

Live imaging was performed as described by Yap et al. (2017). In brief, neurons at DIV 7 were transfected for 36–40 h with the following plasmid combinations: *Nsg1-mCherry* with *Rab7-GFP*, *Nsg1-mCherry* with *Rab7T22N-GFP*, *Nsg1-mCherry* with *GFP*, *mCherry-TFR* with *Rab7-GFP*, *mCherry-TFR* with *Rab7T22N-GFP*, *mCherry-TFR* with *GFP*, *Nsg1-mCherry* with *Rab11-DN-GFP*, *Nsg1-Emerald* with *Rab9-DN-mCherry*, *Rab7-GFP* with *Lamp1-mRFP-Flag*, *Rab7-DN-GFP* with *Lamp1-mRFP-Flag*, and *GFP* with *Lamp1-mRFP-Flag*. Unconjugated transferrin (10 μ g/ml; ChromPure human transferrin; 009-000-050; Jackson ImmunoResearch Laboratories, Inc.) was added to neurons before imaging. Prolong Live Antifade (P36974; Invitrogen) was added right before live imaging. All live imaging was performed on a 37 $^{\circ}$ C heated stage in a chamber with 5% CO₂. All dual and triple live imaging was conducted on an inverted LSM880 confocal microscope using a 40 \times water objective (LD-C Apochromat 1.2W). Images from dual or triple channels were acquired simultaneously with bidirectional scan-frame mode every second for 300–500 frames and with tight gate settings to reduce any overlapping fluor spectra. Laser lines at 488 nm for GFP/Emerald, at 568 nm for mRFP, and at 594 nm for mCherry expression were used. Live imaging for any given set of transfected constructs was repeated in at least five independent cultures. Each time, at least four cells were imaged live. Kymographs were generated using KymographClear (Mangeol et al., 2016) or FIJI (ImageJ; National

Institutes of Health). Events were counted as motile if displacement was $\geq 2 \mu\text{m}$ and otherwise classified as stationary.

WB

Neurons at DIV 10 (~2,000,000 cells) were treated with Leu (20 μM) or CHX (20 $\mu\text{g/ml}$) for the indicated time, washed several times with PBS, and harvested for subcellular fractionation using the BioVision FractionPREP kit following the protocol described by the manufacturer. In brief, cell pellets were resuspended in 100 μl cytosol extraction buffer containing DTT and protease inhibitor cocktail and then incubated on ice for 20 min with gentle mixing every 5 min. Cytosolic fraction was collected after centrifugation at 700 g for 10 min. The remaining pellets were resuspended in 80–100 μl membrane-extraction buffer by vortexing and then incubated on ice for 5 min. Membrane fraction was then collected by centrifugation at 1,000 g for 5 min. The cytosolic and membrane-fractionated samples were subjected to SDS-PAGE and WB analysis using the Odyssey imaging system (LI-COR Biosciences).

Image analysis and quantification

Somatic intensity analysis

10 fields for each condition were analyzed using the Imaris 8.4 image analysis package (Bitplane). In each field, the soma of discernable cells (6–10 per field) were outlined by hand to exclude the nucleus. For the image as a whole, the mean intensity of each marker in these outlined regions was calculated. The values for each field were normalized to the mean of the respective marker minus Leu. Statistics were calculated from the mean values of the 10 images.

Colocalization analysis

Using Imaris 9.0, for each field of view, principal dendrites were identified that could be traced cleanly without interference from other dendrites (total of 17 dendrites). Principal dendrites were masked off MAP2 staining in three different sections, proximal (0–25 μm), juxtaproximal (25–50 μm), and medial (50–75 μm) measured from the edge of the soma. For each marker, a threshold level was determined and used uniformly across all images. Surface objects using the LAMP1 signal were created using the established threshold. These objects were used to create a region of interest, and colocalization of the other markers (CatB and rab7) was determined on a pixel-by-pixel basis by counting as colocalized those pixels which had signal above threshold for both markers.

Abundance and volume analysis

Two different datasets were quantified, both from neurons 7–8 d old. MAP2 was costained against endogenous CatB, LAMP1, and Rab7 and/or against CatD and Nsg2. Using Imaris 9.2, principal (fat) dendrites that were clearly separable from other dendrites were masked off of MAP2 in three different sections, proximal (0–25 μm), juxtaproximal (25–50 μm), and medial (50–75 μm), measured from the edge of the soma. After thresholding the signal such that only signal above background was measured, surface objects for the different markers were created within the individual regions and then counted. The volume of each

region was determined from the volume of the MAP2 mask, and the number of objects divided by the volume of the region was used to determine density. For the volume of the LAMP1 compartments, the same LAMP1 objects created for the abundance analysis were used with the volume calculated by Imaris.

Quantification of Nsg2 endocytosis

Images were quantified for fluorescence intensity in the soma and in the dendrite at time zero and after a 4-h chase using FIJI. Background levels were subtracted for each measurement. For the dendrites, intensity of a line (line width 15), a mean length of 22–30 μm , was drawn at least 15 μm from the soma. The intensity along that line was measured, and then the background was subtracted from it. Values were normalized, and the Kruskal-Wallis test was used to determine significance between groups.

DQ-BSA versus Alexa Fluor 647 ratio determination

The raw intensities of DQ-BSA and Alexa Fluor 647-BSA was determined for each Alexa Fluor 647-BSA⁺ endosome in three different sections, proximal (0–25 μm), juxtaproximal (25–50 μm), and medial (50–75 μm), for 20 major dendrites. The background intensity determined in three areas of the coverslip not containing cells was measured, averaged, and then subtracted for each channel. Ratios of the background-subtracted values of DQ-BSA and Alexa Fluor 647-BSA were then calculated and plotted using Prism (GraphPad Software).

Online supplemental material

Fig. S1 shows the validation of the anti-Rab7 antibody by short hairpin-mediated knockdown in cultured neurons, CatD staining in combination with Rab7 and LAMP1 (all endogenous), and the same data as Fig. 3 D without normalization. Fig. S2 shows Rab7-GFP in combination with endogenous EEA1 and LAMP1. Fig. S3 shows coimaging of Nsg1 endosomes with LysoTracker Red and with active cathepsins using MR-Cat substrates: MR-CatB, MR-CatK, and MR-CatL. Fig. S4 shows how Rab7-DN inhibits degradation of DNER. Fig. S5 shows that Rab9-DN and Rab11-DN do not inhibit the degradation of Nsg2 nor impede the motility of Nsg1 by live imaging.

Acknowledgments

We thank all members of the Winckler laboratory for constructive engagement throughout the duration of this work and critical reading of the manuscript. We gratefully acknowledge the extremely valuable input from Drs. David Castle, Jim Casanova, and Ryan D'Souza (all at University of Virginia, Charlottesville, VA) through many discussions and reading of drafts.

This work was supported by National Institutes of Health grant R01NS083378 (to B. Winckler).

The authors declare no competing financial interests.

Author contributions: C.C. Yap and B. Winckler conceived and coordinated the study and wrote the paper. C.C. Yap carried out all experiments with fixed cells and fractionation for CHX/Leu experiments. C.C. Yap and L. Digilio carried out all live-imaging experiments. L. Digilio carried out all analysis, kymograph preparation, and quantification of videos as well as quantification

of endocytosis chase data. L.P. McMahon performed WB. L.P. McMahon devised and carried out all of the quantitative image analysis using Imaris. A.D.R. Garcia contributed all of the mouse cryosections. C.C. Yap, B. Winckler, L. Digilio, and L.P. McMahon contributed to figure preparation.

Note added in proof. When this paper was in revision, similar observations to ours were made by Cheng et al. (2018. *J. Cell Biol.* <https://doi.org/10.1083/jcb.201711083>) with regard to the heterogeneity of LAMP1-positive compartments. The two studies thus come to the same conclusion that many LAMP1 compartments in axons and dendrites are not degradative.

Submitted: 8 November 2017

Revised: 30 March 2018

Accepted: 31 May 2018

References

Alberi, S., B. Boda, P. Steiner, I. Nikonenko, H. Hirling, and D. Muller. 2005. The endosomal protein NEE21 regulates AMPA receptor-mediated synaptic transmission and plasticity in the hippocampus. *Mol. Cell. Neurosci.* 29:313–319. <https://doi.org/10.1016/j.mcn.2005.03.011>

Barford, K., C.C. Yap, N.D. Dwyer, and B. Winckler. 2017. The related neuronal endosomal proteins NEE21 (Nsg1) and P19 (Nsg2) have divergent expression profiles in vivo. *J. Comp. Neurol.* 525:1861–1878. <https://doi.org/10.1002/cne.24168>

Cai, Q., L. Lu, J.-H. Tian, Y.-B. Zhu, H. Qiao, and Z.-H. Sheng. 2010. Snapin-regulated late endosomal transport is critical for efficient autophagy-lysosomal function in neurons. *Neuron.* 68:73–86. <https://doi.org/10.1016/j.neuron.2010.09.022>

Casanova, J.E., and B. Winckler. 2017. A new Rab7 effector controls phosphoinositide conversion in endosome maturation. *J. Cell Biol.* 216:2995–2997. <https://doi.org/10.1083/jcb.201709034>

Cherry, S., E.J. Jin, M.N. Özel, Z. Lu, E. Agi, D. Wang, W.-H. Jung, D. Epstein, I.A. Meinertzhagen, C.-C. Chan, and P.R. Hiesinger. 2013. Charcot-Marie-Tooth 2B mutations in rab7 cause dosage-dependent neurodegeneration due to partial loss of function. *eLife.* 2:e01064. <https://doi.org/10.7554/eLife.01064>

Cogli, L., F. Piro, and C. Bucci. 2009. Rab7 and the CMT2B disease. *Biochem. Soc. Trans.* 37:1027–1031. <https://doi.org/10.1042/BST0371027>

Cornejo, V.H., A. Luarte, and A. Couve. 2017. Global and local mechanisms sustain axonal proteostasis of transmembrane proteins. *Traffic.* 18:255–266. <https://doi.org/10.1111/tra.12472>

Dauth, S., R.F. Sîrbulescu, S. Jordans, M. Rehders, L. Avena, J. Oswald, A. Lerchl, P. Saftig, and K. Brix. 2011. Cathepsin K deficiency in mice induces structural and metabolic changes in the central nervous system that are associated with learning and memory deficits. *BMC Neurosci.* 12:74. <https://doi.org/10.1186/1471-2202-12-74>

De Luca, M., L. Cogli, C. Progidia, V. Nisi, R. Pascolutti, S. Sigismund, P.P. Di Fiore, and C. Bucci. 2014. RILP regulates vacuolar ATPase through interaction with the VIG1 subunit. *J. Cell Sci.* 127:2697–2708. <https://doi.org/10.1242/jcs.142604>

Ding, X., W. Zhang, T. Zhao, C. Yan, and H. Du. 2017. Rab7 GTPase controls lipid metabolic signaling in myeloid-derived suppressor cells. *Oncotarget.* 8:30123–30137.

Douglas, P.M., and A. Dillin. 2010. Protein homeostasis and aging in neurodegeneration. *J. Cell Biol.* 190:719–729. <https://doi.org/10.1083/jcb.201005144>

Ehlers, M.D. 2000. Reinsertion or degradation of AMPA receptors determined by activity-dependent endocytic sorting. *Neuron.* 28:511–525. [https://doi.org/10.1016/S0896-6273\(00\)00129-X](https://doi.org/10.1016/S0896-6273(00)00129-X)

Eiraku, M., Y. Hirata, H. Takeshima, T. Hirano, and M. Kengaku. 2002. Delta/notch-like epidermal growth factor (EGF)-related receptor, a novel EGF-like repeat-containing protein targeted to dendrites of developing and adult central nervous system neurons. *J. Biol. Chem.* 277:25400–25407. <https://doi.org/10.1074/jbc.M110793200>

Eiraku, M., A. Tohgo, K. Ono, M. Kaneko, K. Fujishima, T. Hirano, and M. Kengaku. 2005. DNER acts as a neuron-specific Notch ligand during

Bergmann glial development. *Nat. Neurosci.* 8:873–880. <https://doi.org/10.1038/nn1492>

Fariás, G.G., C.M. Guardia, R. De Pace, D.J. Britt, and J.S. Bonifacino. 2017. BORC/kinesin-1 ensemble drives polarized transport of lysosomes into the axon. *Proc. Natl. Acad. Sci. USA.* 114:E2955–E2964. <https://doi.org/10.1073/pnas.1616363114>

Fernández-Monreal, M., T.C. Brown, M. Royo, and J.A. Esteban. 2012. The balance between receptor recycling and trafficking toward lysosomes determines synaptic strength during long-term depression. *J. Neurosci.* 32:13200–13205. <https://doi.org/10.1523/JNEUROSCI.0061-12.2012>

Goo, M.S., L. Sancho, N. Slepak, D. Boassa, T.J. Deerinck, M.H. Ellisman, B.L. Bloodgood, and G.N. Patrick. 2017. Activity-dependent trafficking of lysosomes in dendrites and dendritic spines. *J. Cell Biol.* 216:2499–2513. <https://doi.org/10.1083/jcb.201704068>

Gowrishankar, S., P. Yuan, Y. Wu, M. Schrag, S. Paradise, J. Grutzendler, P. De Camilli, and S.M. Ferguson. 2015. Massive accumulation of luminal protease-deficient axonal lysosomes at Alzheimer's disease amyloid plaques. *Proc. Natl. Acad. Sci. USA.* 112:E3699–E3708. <https://doi.org/10.1073/pnas.1510329112>

Gowrishankar, S., Y. Wu, and S.M. Ferguson. 2017. Impaired JIP3-dependent axonal lysosome transport promotes amyloid plaque pathology. *J. Cell Biol.* 216:3291–3305. <https://doi.org/10.1083/jcb.201612148>

Guerra, F., and C. Bucci. 2016. Multiple Roles of the Small GTPase Rab7. *Cells.* 5:34. <https://doi.org/10.3390/cells5030034>

Hubert, V., A. Peschel, B. Langer, M. Gröger, A. Rees, and R. Kain. 2016. LAMP-2 is required for incorporating syntaxin-17 into autophagosomes and for their fusion with lysosomes. *Biol. Open.* 5:1516–1529. <https://doi.org/10.1242/bio.018648>

Humphries, W.H., C.J. Szymanski, and C.K. Payne. 2011. Endo-Lysosomal Vesicles Positive for Rab7 and LAMP1 Are Terminal Vesicles for the Transport of Dextran. *PLoS One.* 6:e26626.

Huotari, J., and A. Helenius. 2011. Endosome maturation. *EMBO J.* 30:3481–3500. <https://doi.org/10.1038/emboj.2011.286>

Jin, E.J., F.R. Kiral, and P.R. Hiesinger. 2017. The where, what, and when of membrane protein degradation in neurons. *Dev. Neurobiol.* 78:283–297.

Jin E.J., Kiral, F.K., Özel, M.N., Burchardt, L.S., Osterland, M., Epstein, D., Wolfenberger, H., Prohaska, S., and Hiesinger, P.R. (2018). Live Observation of Two Parallel Membrane Degradation Pathways at Axon Terminals. *Curr. Biol Apr 2;28(7):1027-1038.e4* <https://doi.org/10.1016/j.cub.2018.02.032>

Johnson, D.E., P. Ostrowski, V. Jaumouillé, and S. Grinstein. 2016. The position of lysosomes within the cell determines their luminal pH. *J. Cell Biol.* 212:677–692. <https://doi.org/10.1083/jcb.201507112>

Kawauchi, T., K. Sekine, M. Shikanai, K. Chihama, K. Tomita, K. Kubo, K. Nakajima, Y. Nabeshima, and M. Hoshino. 2010. Rab GTPases-dependent endocytic pathways regulate neuronal migration and maturation through N-cadherin trafficking. *Neuron.* 67:588–602. <https://doi.org/10.1016/j.neuron.2010.07.007>

Kim, T., Y. Yamamoto, and K. Tanaka-Yamamoto. 2017. Timely regulated sorting from early to late endosomes is required to maintain cerebellar long-term depression. *Nat. Commun.* 8:401. <https://doi.org/10.1038/s41467-017-00518-3>

Lasiecka, Z.M., C.C. Yap, J. Katz, and B. Winckler. 2014. Maturation conversion of dendritic early endosomes and their roles in L1-mediated axon growth. *J. Neurosci.* 34:14633–14643. <https://doi.org/10.1523/JNEUROSCI.1837-14.2014>

Lee, S., Y. Sato, and R.A. Nixon. 2011. Lysosomal proteolysis inhibition selectively disrupts axonal transport of degradative organelles and causes an Alzheimer's-like axonal dystrophy. *J. Neurosci.* 31:7817–7830. <https://doi.org/10.1523/JNEUROSCI.6412-10.2011>

Liu, H., and C. Wu. 2017. Charcot Marie Tooth 2B Peripheral Sensory Neuropathy: How Rab7 Mutations Impact NGF Signaling? *Int. J. Mol. Sci.* 18:324. <https://doi.org/10.3390/ijms18020324>

Liu, K., R. Xing, Y. Jian, Z. Gao, X. Ma, X. Sun, Y. Li, M. Xu, X. Wang, Y. Jing, et al. 2017. WDR91 is a Rab7 effector required for neuronal development. *J. Cell Biol.* 216:3307–3321. <https://doi.org/10.1083/jcb.201705151>

Maday, S., and E.L.F. Holzbaur. 2016. Compartment-Specific Regulation of Autophagy in Primary Neurons. *J. Neurosci.* 36:5933–5945. <https://doi.org/10.1523/JNEUROSCI.4401-15.2016>

Mangeol, P., B. Prevot, and E.J.G. Peterman. 2016. KymographClear and KymographDirect: two tools for the automated quantitative analysis of molecular and cellular dynamics using kymographs. *Mol. Biol. Cell.* 27:1948–1957. <https://doi.org/10.1091/mbc.e15-06-0404>

Norstrom, E.M., C. Zhang, R. Tanzi, and S.S. Sisodia. 2010. Identification of NEE21 as a β -amyloid precursor protein-interacting protein in vivo

- that modulates amyloidogenic processing in vitro. *J. Neurosci.* 30:15677–15685. <https://doi.org/10.1523/JNEUROSCI.4464-10.2010>
- Padamsey, Z., L. McGuinness, S.J. Bardo, M. Reinhart, R. Tong, A. Hedegaard, M.L. Hart, and N.J. Emptage. 2017. Activity-Dependent Exocytosis of Lysosomes Regulates the Structural Plasticity of Dendritic Spines. *Neuron.* 93:132–146. <https://doi.org/10.1016/j.neuron.2016.11.013>
- Parton, R.G., K. Simons, and C.G. Dotti. 1992. Axonal and dendritic endocytic pathways in cultured neurons. *J. Cell Biol.* 119:123–137. <https://doi.org/10.1083/jcb.119.1.123>
- Pols, M.S., E. van Meel, V. Oorschot, C. ten Brink, M. Fukuda, M.G. Swetha, S. Mayor, and J. Klumperman. 2013. hVps41 and VAMP7 function in direct TGN to late endosome transport of lysosomal membrane proteins. *Nat. Commun.* 4:1361. <https://doi.org/10.1083/ncomms2360>
- Ponomareva, O.Y., K.W. Eliceiri, and M.C. Halloran. 2016. Charcot-Marie-Tooth 2b associated Rab7 mutations cause axon growth and guidance defects during vertebrate sensory neuron development. *Neural Dev.* 11:2. <https://doi.org/10.1186/s13064-016-0058-x>
- Rink, J., E. Ghigo, Y. Kalaidzidis, and M. Zerial. 2005. Rab conversion as a mechanism of progression from early to late endosomes. *Cell.* 122:735–749. <https://doi.org/10.1016/j.cell.2005.06.043>
- Schwenk, B.M., C.M. Lang, S. Hög, S. Tahirovic, D. Orozco, K. Rentzsch, S.F. Lichtenthaler, C.C. Hoogenraad, A. Capell, C. Haass, and D. Edbauer. 2014. The FTL risk factor TMEM106B and MAP6 control dendritic trafficking of lysosomes. *EMBO J.* 33:450–467.
- Stahl, S., Y. Reinders, E. Asan, W. Mothes, E. Conzelmann, A. Sickmann, and U. Felbor. 2007. Proteomic analysis of cathepsin B- and L-deficient mouse brain lysosomes. *Biochim. Biophys. Acta.* 1774:1237–1246. <https://doi.org/10.1016/j.bbapap.2007.07.004>
- Steiner, P., J.C. Sarria, L. Glauser, S. Magnin, S. Catsicas, and H. Hirling. 2002. Modulation of receptor cycling by neuron-enriched endosomal protein of 21 kD. *J. Cell Biol.* 157:1197–1209. <https://doi.org/10.1083/jcb.200202022>
- Steiner, P., S. Alberi, K. Kulangara, A. Yersin, J.-C.F. Sarria, E. Regulier, S. Kasas, G. Dietler, D. Muller, S. Catsicas, and H. Hirling. 2005. Interactions between NEEP21, GRIP1 and GluR2 regulate sorting and recycling of the glutamate receptor subunit GluR2. *EMBO J.* 24:2873–2884. <https://doi.org/10.1038/sj.emboj.7600755>
- Vanlandingham, P.A., and B.P. Ceresa. 2009. Rab7 regulates late endocytic trafficking downstream of multivesicular body biogenesis and cargo sequestration. *J. Biol. Chem.* 284:12110–12124. <https://doi.org/10.1074/jbc.M809277200>
- Wang, T., Z. Ming, W. Xiaochun, and W. Hong. 2011. Rab7: role of its protein interaction cascades in endo-lysosomal traffic. *Cell. Signal.* 23:516–521. <https://doi.org/10.1016/j.cellsig.2010.09.012>
- Yap, C.C., D. Wisco, P. Kujala, Z.M. Lasiecka, J.T. Cannon, M.C. Chang, H. Hirling, J. Klumperman, and B. Winckler. 2008. The somatodendritic endosomal regulator NEEP21 facilitates axonal targeting of LI/NgCAM. *J. Cell Biol.* 180:827–842. <https://doi.org/10.1083/jcb.200707143>
- Yap, C.C., L. Digilio, L. McMahon, and B. Winckler. 2017. The endosomal neuronal proteins Nsg1/NEEP21 and Nsg2/P19 are itinerant, not resident proteins of dendritic endosomes. *Sci. Rep.* 7:10481. <https://doi.org/10.1038/s41598-017-07667-x>